Ancient Martian aeolian sand dune deposits recorded in the stratigraphy of Valles Marineris and implications for past climates

Matthew Chojnacki*[1,2], Lori K. Fenton[3], Aaron Robert Weintraub[4], Lauren A. Edgar[5]
Mohini J. Jodhpurkar[5], & Christopher S. Edwards[4].

[1]Planetary Science Institute, Tucson, AZ

[2]Lunar and Planetary Lab, University of Arizona, Tucson, AZ

[3]Carl Sagan Center, SETI Institute, Mountain View, CA

[4]Northern Arizona University, Department of Astronomy and Planetary Science, Flagstaff, AZ

[5]U.S. Geological Survey, Astrogeology Science Center, Flagstaff, AZ

*Corresponding Author:

Matthew Chojnacki

Planetary Science Institute,

1700 East Fort Lowell

Tucson, AZ 85719-2395 USA

Phone: 720-635-8596

Email: mchojnacki@psi.edu

Key Points:

- Sedimentary deposits were identified in Valles Marineris and interpreted as ancient aeolian dune fields with a range of preservation states
- Their preservation indicates a complex history with periods of migration, burial, stabilization, cementation, exhumation, and erosion
- Paleo-dune morphologies compared with modern indicators suggest no major shifts in wind regime have occurred since their stabilization

Descriptive headings for each section:

1. Introduction and motivation – introduction and motivation for the study, including a broad overview of aeolian bedforms in the terrestrial and Martian geologic record.

2. Study region – a brief description of the Valles Marineris environment and geologic record.

3. Overview of approach datasets and methods – details for our approach that include our paleo-bedform identification criteria and various datasets used to constrain their properties and geologic history.

4. Results – a description of paleo-bedforms in the study area including their geologic context, thermophysical & compositional properties, comparison to modern dune fields, and relation to the modern wind regime(s).

5. Discussion: synthesis of results and implications – the interpretations of our results with a discussion related to constraints on paleo-wind regime(s), paleo-dune ages, and a proposed sequence of events that led to their presevation and exposure.

6. Conclusions: a summary of results and their possible implications.

ABSTRACT

Aeolian sediment transport, deposition, and erosion have been ongoing throughout Mars' history. This record of widespread aeolian processes is preserved in landforms and geologic units that retain important clues about past environmental conditions including wind patterns. In this study we describe landforms within Melas Chasma, Valles Marineris, that occur in distinct groups with linear to crescentic shapes, arranged with a characteristic wavelength; some possess slope profiles analogous to modern sand dunes, yet show evidence for lithification. Based on the features' dimensions, asymmetry, and spatial patterns relative to modern equivalents, we interpret these landforms to be two classes of aeolian bedforms: decameter-scale mega-ripples and sand dunes. The presence of superposed erosional features and depositional units indicates these landforms were cemented and likely ancient. Melas paleo-dunes are found atop Hesperian-aged layered deposits, but we estimate them to be younger, likely lithified in the Amazonian period. Although a range of degradation was observed, some paleo-dunes are >10 m tall and maintain steep lee sides (>25°), an uncommon scenario for terrestrial examples as other geologic processes lead to dune obliteration. The preserved paleo-bedform geometries are largely consistent with those of modern aeolian indicators, suggesting no major shifts in wind regime or contributing boundary conditions. Finally, we propose their appearance and context require sequential periods of dune migration, stabilization following catastrophic burial, cementation, differential erosion, exposure, and burial. The presence of wholly preserved duneforms appears to be more common on Mars compared to the Earth and may signal something important about Martian landscape evolution.

Plain Language Summary

Wind-driven sand dunes are common on modern Mars and the presence of certain sedimentary rock layers indicates these landforms occurred there in the past. Here, we explore features in the canyons of Valles Marineris which show characteristics frequently attributed to dunes, yet evidence for their lithification and burial is clear. Their horizontal extent, height, shape, slopes, and collective spatial patterns led to our interpretation of them as lithified dune fields. The heavily eroded appearance along with superposed elements such as craters and boulders led to the conclusion that these are relatively ancient landforms. Despite this erosion This level of preservation is rare for terrestrial sand dunes due to erosion and tectonics, thus providing an opportunity to reconstruct the various factors contributing to their history. Understanding the circumstances that led to the preservation of these ancient duneforms will yield crucial information regarding planetary sedimentary processes and the geologic history of the region.

1.0 Introduction and motivation

Sedimentary rocks on Mars attest to a variety of aqueous and atmospheric processes throughout its history. For example, rover investigations at Meridiani Planum and Gale crater have firmly established that some of the ~3.7 Ga rock record is composed of sediment that was transported by flowing wind and water, as evidenced by abundant cross-bedding and fine layering (Squyres et al., 2009; Edgar et al., 2012, 2018; Grotzinger et al., 2012; Banham et al., 2018). Across the surface other isolated occurrences that meet the morphologic criteria for dunes and ripples are evident in orbital data, yet appear degraded and eroded (e.g., Edgett & Malin, 2000; Burr et al., 2004; Durrant et al., 2017). Although full preservation of bedforms on Earth is uncommon, the presence of impact craters and blocks on the surface of these bedforms suggests they are well lithified (Greeley & Iversen, 1985; Kocurek & Ewing, 2012). Understanding the physical properties and conditions that contributed to the formation and preservation of these anomalous landforms will yield crucial information regarding sedimentary processes on Mars and their contributions to the rock record.

Partially preserved ancient bedforms on Mars were reported earlier by Edgett and Malin (2000) based on orbital image analysis of Apollinaris Sulci. That study described a field of moderate albedo, crescent-shaped features with superposed craters that were interpreted as exhumed paleo-dune field deposits (Edgett & Malin, 2000; their Fig. 23b). Similar, yet rare, scenarios have occurred on Earth in which dune fields were rapidly flooded by lava or water, which led to the preservation of dune morphologies (e.g., Mountney et al., 1999; Ahmed Benan & Kocurek, 2000; Jerram et al., 2000; Waichel et al., 2008). Some of these remarkable examples include largely intact stoss-to-lee morphologies of barchan and transverse dunes (Jerram et al., 2000; Waichel et al., 2008). Without such events complete stoss and lee slopes of terrestrial bedforms are rarely preserved to such a high degree. Limited dune preservation occurs largely as a result of bedform climbing as successive dunes first scour the surfaces of dune deposits on which they encroach, often leaving behind only the basal 10-20% of dunes (Rubin & Hunter, 1982; Kocurek, 1991). Other processes common on Earth but rare or absent for most of Mars' history, such as aqueous erosion, tectonics, and vegetation, also contribute to dune obliteration. Evidence for a large-scale, non-destructive preservation process for Martian dunes provides an opportunity to study the various geologic events which may have contributed to their preservation. Moreover, well-preserved, cemented bedforms that retain their gross morphology allow ancient wind regimes to be reconstructed and compared with modern aeolian indicators.

In this study we explore hypothesized landforms on Mars, termed "paleo- bedforms." These newly documented linear to crescentic, positive-relief features of a characteristic wavelength, which are inferred to have formed by aeolian processes, are found in Valles Marineris (see Section 2). To examine their geomorphology, we utilized High Resolution Imaging Science Experiment (HiRISE; McEwen et al., 2007) images and derived topography (see Section 3). Here, we seek to address key questions related to the nature of ancient bedform formation and their subsequent modification history. The objectives of this paper are to (i) document the bedform properties and spectral characteristics of paleo-bedforms in Melas Chasma, (ii) identify the processes by which these bedforms were preserved, (iii) constrain the geologic periods in which paleo-bedforms formed, and (iv) infer paleo-flow regimes based on local and regional paleo-bedform morphology.

2.0 Study Region

A prior global survey using HiRISE data revealed a wide distribution of areas hosting candidate paleo-bedforms in various geographic contexts (e.g. craters, basins) (Chojnacki et al., 2018b). One of the most promising regions with well-preserved paleo-bedforms is within Valles Marineris. Specifically, this study focuses on several deposits in Melas Chasma (10°S–14°S, 284°E–290°E; Fig. 1). Melas Chasma offers a range of paleo-bedform preservation states with relatively dust-free surfaces that allow for spectral investigations.

Melas Chasma is located in central Valles Marineris, bounded by Noachian-aged wall rock units consisting of massive spur and gully formations, and undivided floor units from the

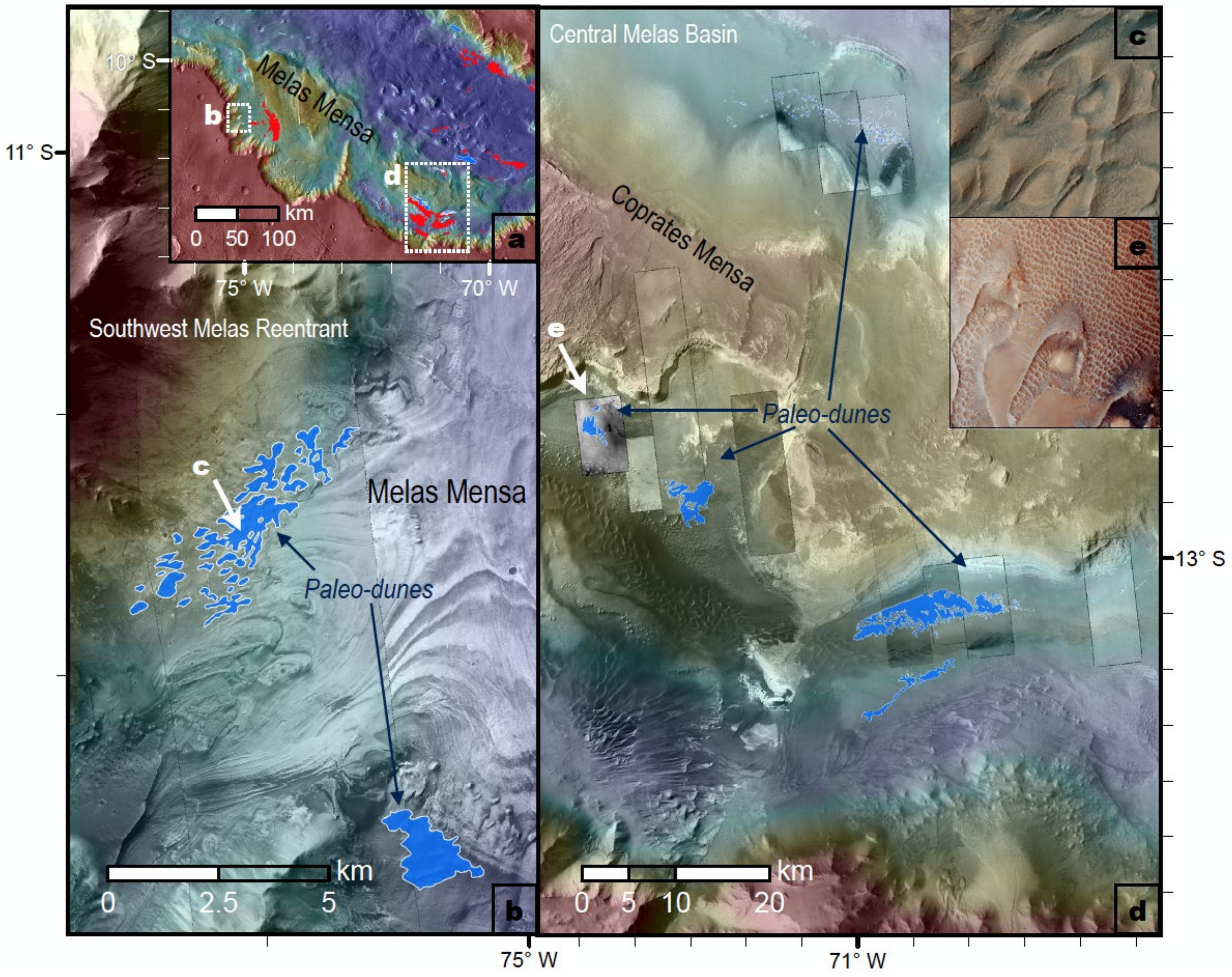

Figure 1. Context maps for Melas Chasma paleo-dune fields. Base maps are CTX mosaics colorized with MOLA elevation from +2 to -4 km. Secondary lat/long tick marks are 1/10°. (a) Regional distribution of paleo- (blue polygons outlined in white) and modern (red polygons) dune fields. (b) Southwest Melas Chasma reentrant canyon and the (d) central basin of Melas Chasma. HiRISE examples of select dunes with (c) ESP_025666_1685 and (e) ESP_025666_1685. Images are ~750 m wide and locations marked with white arrows. All images are oriented north up unless indicated. CTX mosaic data courtesy Murray Lab/Caltech/MSSS/JPL.

Noachian-Hesperian transition period (Tanaka et al., 2014). Basin floor units largely consist of prominent light-toned sedimentary layered deposit mounds and lower-lying basin fill. The canyon interiors comprise numerous geologic units of various terrain ages and origins (e.g., alluvial fans, structural massifs, lava flows) (Okubo, 2010; Fortezzo et al., 2016; Davis et al., 2018). Surficial units of dark-toned capping mantle materials and low albedo sand dunes are common to the study area (Weitz et al., 2012; Chojnacki et al., 2014a). Meter-scale dark-toned sand ripples and decameter-scale bright-toned bedforms known as Transverse Aeolian Ridges (TARs) (Bourke et al., 2003) are also common to these areas, often filling topographic lows (Williams & Weitz, 2014; Chojnacki et al., 2018a).

3.0 OVERVIEW OF APPROACH DATASETS AND METHODS

Candidate paleo-bedform sites were surveyed to document their key characteristics, with the ultimate goal of constraining the processes responsible for their preservation. This survey employed a variety of remote sensing data and techniques.

3.1 Paleo-bedform identification criteria

For the purposes of this study, candidate remnant aeolian bedforms were defined by meeting the following criteria:

1) possess the morphology of a whole or part a bedform, and

2) show characteristics indicative of long-term induration.

Bedforms are identified (criterion 1) as distinct groups of repeating, linear to crescentic landforms of a characteristic wavelength and consistent orientation (for unidirectional flow), and possess low sinuosity, while displaying branching and merging patterns (Bagnold, 1941; Lancaster, 2009; Kocurek et al., 2010). The bifurcation of crestlines is key to the interpretation of linear duneforms; these defects are universally recognized in bedforms formed in a variety of subaqueous and subaerial environments (Anderson & McDonald, 1990; Milliken et al., 2014). Crescent-shaped dunes (e.g., barchan, barchanoid, or dome) are particularly common on Mars and may be identified based on their elongated horns and asymmetric profiles (Bourke, 2010).

Other Martian landforms can resemble the gross morphology of bedforms leading to incorrect attribution. Glacial terrain (Banks et al., 2008), volcanic lava textures (e.g., festoon ridges) (Keszthelyi et al., 2008), and aeolian erosional yardangs (Kerber & Head, 2010), may resemble paleo-dunes. These landforms and terrain all come with distinguishing characteristics and contexts that often deviate from subaqueous and subaerial depositional bedforms. Regardless, issues relating to equifinality were considered by utilizing multiple criteria and exploring other possible formation mechanisms.

To identify bedforms as inactive and possibly ancient (criterion 2), the following morphologic criteria may be apparent in HiRISE data: 1) features or landforms that superpose the bedform (e.g., craters, boulders, boulder tracks, lava flows, or landslides); 2) morphologic evidence for erosion in the form of fracturing of bedform slopes and associated colluvium (e.g., scree or talus); and 3) the nighttime thermal inertia of candidate locations may be higher than is possible for unconsolidated sand (>350–400 $Jm^{-2}K^{-1}s^{-1/2}$) (Christensen, 1983; Fergason et al., 2006; Edwards et al., 2018). The last condition is not a mandatory criterion as even a relatively thin layer of surficial dust or lateral mixing of loose particulate (e.g., regolith) can lower the overall thermal inertia (Edwards et al., 2018).

3.2 Surface morphology: Visible-wavelength images

To identify photogeologic evidence of paleo-bedforms and characterize their morphology, we utilized images from the Context Camera (CTX) (Malin et al., 2007) at 5–6 m/pixel and the HiRISE camera at 25–50 cm/pixel both onboard the Mars Reconnaissance Orbiter (MRO).

HiRISE-enhanced color images were also used to assess meter-scale variations in color and inferred composition as these products can reveal subtle variations in ferrous vs. ferric iron concentrations (Delamere et al., 2010). See Table S1 for image information.

3.3 Topography: digital elevation models and slope maps

To measure topographic relationships between paleo-bedforms and neighboring geologic units (e.g., maximum gradient, relative elevations), we employed two types of digital terrain models (DTMs). To investigate fine-scale surface topography and slopes, HiRISE DTMs (1 m/post) and orthoimages of paleo-dune fields were constructed using SOCET SET® BAE system photogrammetry software (see supporting information section 1 for more details and Table S1 for DTMs) (Kirk et al., 2008). HiRISE slope maps at ~3-5 m baselines were derived from DTMs using in-house code that runs a 3x3 low-pass filter on the terrain 3 times (Fig. S1).Gridded regional topographic elevation data from the Mars Orbiter Laser Altimeter (MOLA) were used for regional context (Smith et al., 2001).

3.4 Stratigraphy and geologic relationships: geologic mapping

Geologic maps of select areas were constructed through digital mapping at ~1:2,000 scale using HiRISE and CTX basemaps, to produce maps at 1:10,000 scale. This scale was selected based on the small size of the landforms (~100s of meters) and available datasets. Mapping was performed using Esri's ArcGIS® 10 software. Geologic units were identified based on tone, texture, and morphology, whereas stratigraphic associations were determined through crosscutting relationships.

3.5 Thermophysical and compositional properties: thermal inertia and spectra

Thermal inertia (TI) was used to understand the physical properties of candidate paleo-bedforms. Materials with high porosity, such as sand, have inefficient heat flow and low thermal conductivity leading to low TI. For more consolidated materials, where heat can flow through larger grain-to-grain boundaries more efficiently, thermal conductivity and TI are higher.

The KRC thermal model (Kieffer, 2013) was used to derive TI values of candidate paleo-bedform fields from band 9 (12.57 μm) pre-sunrise data from the Thermal Imaging System (THEMIS) on board the Mars Odyssey spacecraft (Christensen et al., 2004; Fergason, Christensen,

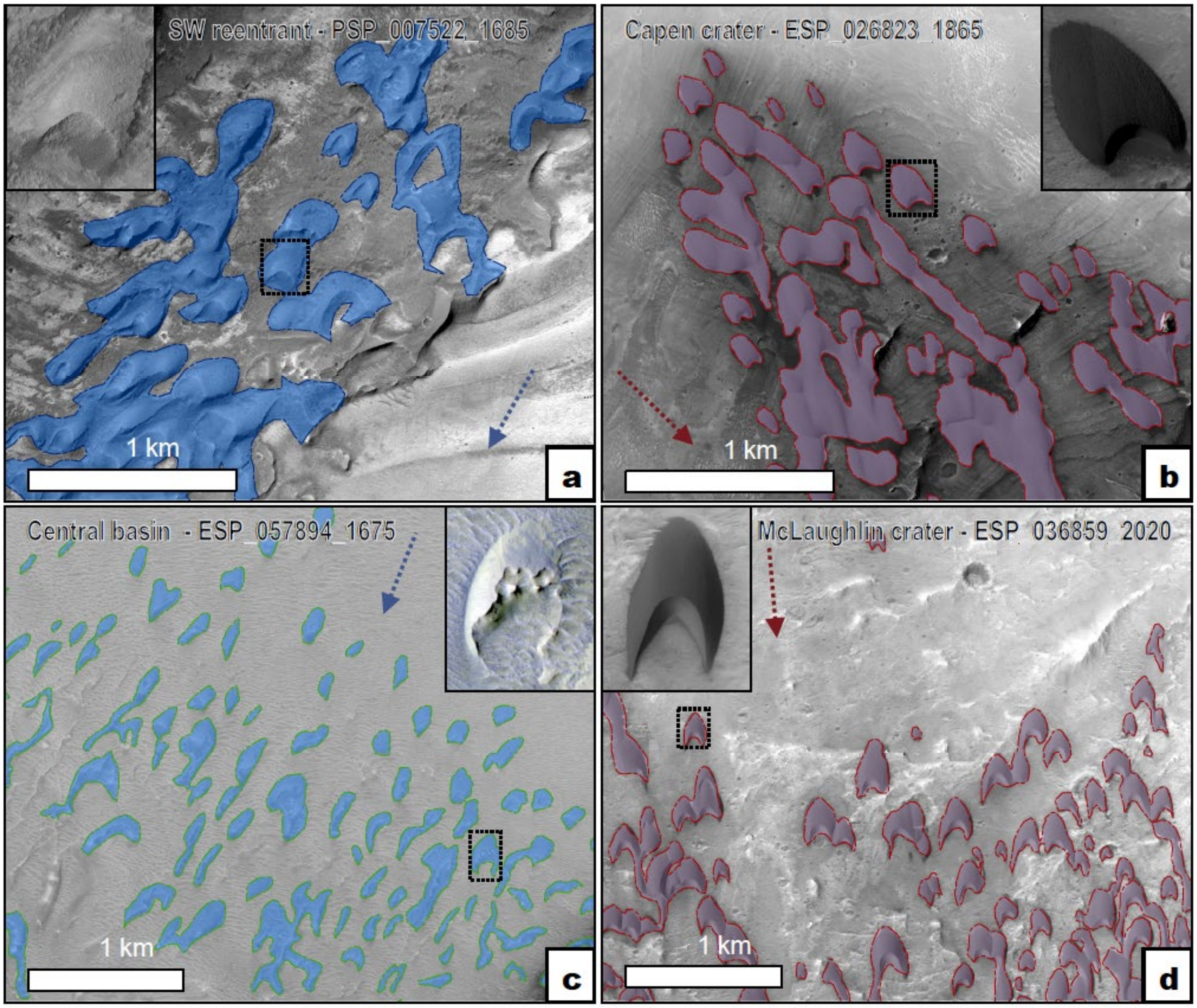

Figure 2. Geomorphic and spatial comparisons of paleo- (cyan polygons) and (magenta polygons) modern dune fields with dashed arrows for interpreted wind directions at the same scale in HiRISE images. (a) Southwest Melas reentrant canyon (field 2849-111; 284.9°E, 11.1°S) in comparison with (b) modern dunes in Capen crater (14.3°E, 6.4°N). (c) Central Melas basin (field 2891-122; 289.1°E, 12.2°S) in comparison with (d) modern dunes in McLaughlin crater (337.6°E, 21.9°N). Insets show HiRISE examples of select dunes at the same scale (widths are ~240 m).

& Kieffer, 2006). Using THEMIS brightness temperature images (100 m/pixel) and additional parameters (e.g., slope, elevation, albedo, dust opacity), a thermal inertia lookup table (in units of $Jm^{-2}K^{-1}s^{-1/2}$ or thermal inertia units, TIUs) was generated corresponding to known temperatures (Edwards et al., 2018) and interpolated to the best fit TI. This methodology allows for pixel-by-pixel TI derivation and was devised by Edwards et al. (2018) through ground-truthing of THEMIS-derived TI to the *Curiosity* rover-derived TI. See supporting information section 2.

Spectral data from MRO's Compact Reconnaissance Imaging Spectrometer for Mars (CRISM; Murchie et al., 2007, 2009) were used to characterize paleo-bedform field mineralogy. Full-Resolution Targeted (FRT) data (18 m/pixel and 545 spectral bands) were used for this study, allowing for near-complete spectral characterization over the visible/near-infrared and shortwave infrared region. Spectra from regions of interest (ROI) were divided by spectrally bland regions, within the same pixel columns from un-projected images, to highlight differences between the paleo-bedforms and their adjacent units. Spectral processing for photometric and atmospheric corrections followed established standards by the CRISM team (Murchie et al., 2007; McGuire et al., 2009). See supporting information section 2.

4.0 Results

This section describes the morphology, stratigraphy, geologic context, and interpretation of candidate paleo-bedforms found within Melas Chasma. Subsequent sections report results related to paleo-bedform thermophysical properties, composition, and relation to modern wind indicators.

4.1 Southwest Melas Chasma reentrant paleo-bedform morphology and geology

Description: Two large concentrations (covering a total area of ~6.5 km^2) of broadly crescentic, positive-relief features are located between several prominent wall spurs that extend downslope at

Table 1. Geomorphology and thermophysical properties of paleo-dune and modern dunes with uncertainty of ±1σ. Measurements are in units of meters unless otherwise noted.

Name and Site ID[a]	SW Melas reentrant 2849-111	C Melas basin 2891-122	S Melas Mensa 2892-131	C Melas basin 2895-119	S Melas Mensa 2886-129	Capen crater 0141+063	McLaughlin crater 3373+216
Measurements	25	8	10	5	5	13	15
Degradation State[b]	1-2	1-3	1-3	Modern	Modern	Modern	Modern
Wavelength	380±113	400±79	363±177	440±200	-	272±56	322±178
Height	7.6±3.2	11.3±4.1	12.9±3.2	23.8±12.3	-	10.0±2.7	17.9±7.7
Length	171±31	238±55	208±83	221±103	-	166±31	151±53
Dune field area (km^2)	6.5	5.9	35.9	13.1	419.5	96.8	142.0
Thermal Inertia (TIU)	296±18	166±18	226±17	249±15	271±18	382±37	370±36

[a] Dune field site IDs, where the first four digits are the monitoring site's centroid east longitude, the last three digits are the site's latitude (each coordinate given to the first decimal place without the decimal), and the separating + or – sign indicating which hemisphere. See Table S1 for relevant HiRISE data information.

[b] Degradation state is a qualitative metric (1-3) where endmembers are (1) largely preserved, weakly lithified, sparsely cratered bedforms, compared with (3) poorly preserved, heavily pitted, possibly partially buried, landforms with characteristic consistent with bedforms.

5-10° into the central canyon area, hereafter termed Southwest Melas reentrant (Fig. 1b). These landforms resemble barchan dunes, some with elongated arcuate facets pointing upslope towards the southwest, whereas others show less symmetric crescentic shapes. These 171±31 m-long, 7.6±3.2 m tall landforms are spaced with crest-to-crest wavelengths ranging from ~250-500 m—similar to many modern Martian barchan dunes (Table 1; Fig. 2; see section 4.3). These features exhibit a consistent northeast-southwest asymmetry in which their southwest slopes (15-25°) are notably steeper than their northeast-facing slopes (5-15°; Fig. S1a). Their surfaces are variably eroded and superposed by pits, boulders, fractures, and minor accumulations of talus at the base of steeper slopes (Fig. 3). Only a few small (decameter-sized) craters were identified directly on candidate paleo-bedforms, indicating a relatively young surface exposure age (Fig. 3, S2).

Interpretation: Based on the spatial patterns, wavelength, height, asymmetry, and presence of superimposed boulders and craters, we infer that these landforms record ancient barchan and

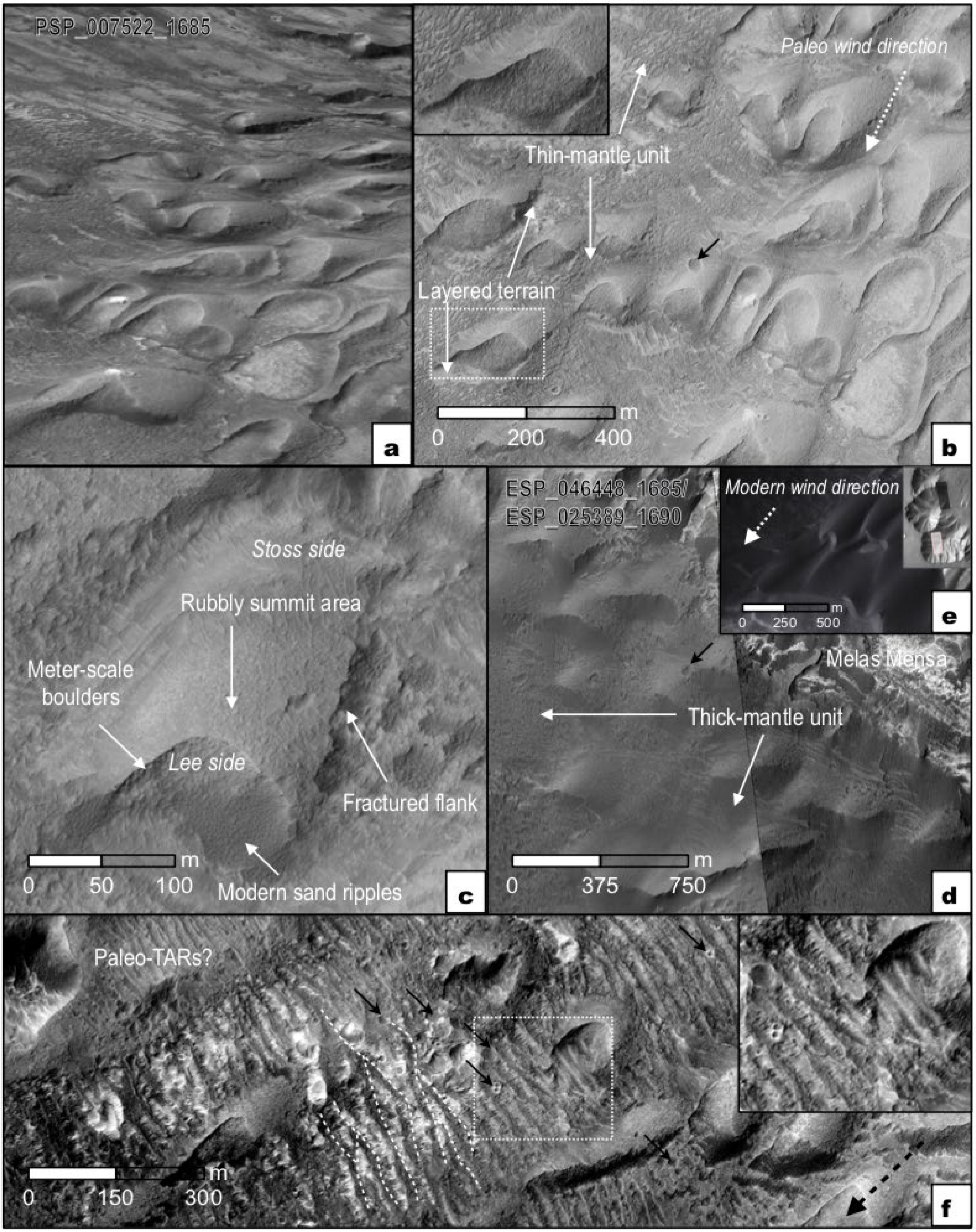

Figure 3. Geomorphology of the Southwest Melas reentrant area paleo-dunes (field 2849-111). See Fig. 6a for image locations. (a) Oblique view of site from the south-southeast where the field of view is ~800 m across and vertical exaggeration is ~2X. (b) Central areas with a (inset) closer view of paleo-dune and mantle units, including a small superposed crater (black arrow) and interpreted wind direction (dashed arrow). (c) A detailed view of one paleo-dune and signs of its degradation. (d) Partially buried paleo-dunes by thicker mantle units to the southeast. (e) Comparison with modern dunes in the adjacent canyon to the south (HiRISE ESP_047015_1685). (inset) THEMIS image showing locations of paleo- (black box) and modern (white box) dunes. (f) Parallel rows of dark resistant ridges at 15−50 meter spacings, which are candidate ancient mega-ripples or TARs. These features are oriented perpendicular to the dune field axis (dashed white arrow) and bifurcate in some areas (dashed white lines). Note the superposed impact craters (black arrows). See Fig. S2 for location and topographic profiles.

barchanoid dunes. Gently dipping northeast-facing slopes are inferred to represent stoss slopes, while the steeper southwest-facing slopes are inferred to represent lee slopes. These latter areas are not likely preserved crests, rather they are remnants of dune summit sections. In some cases, slopes above the angle of repose for fine granular material (~30-35° or steeper; Atwood-Stone and McEwen, 2013; Ewing et al., 2017) are observed on flanks or lee sides (Fig. S1). This indicates a strong cementing agent has lithified the sand as these steep slopes would be most susceptible to mass wasting. The scale, shape, and the upslope paleo-transport direction indicate these landforms formed in an aeolian, rather than a subaqueous environment.

The geologic map of this area reveals these paleo-dunes are not directly onlapping Noachian-aged wall units/rocks, rather they onlap younger sedimentary strata of Melas Mensa (Fig. 4b). Noachian wall rock is overlain by Hesperian layered deposits, some bearing hydrated sulfates (Liu et al., 2018). The layered deposits are in turn overlain by paleo-dunes, which argue for a younger age. A distinct, moderately eroded dark-toned unit of variable thickness (~1-10 m) onlaps many paleo-dunes and other units. Another group of crescentic features to the southeast has a nearly identical orientation but is partially buried by mantle material (Fig. 3d, 3f, 4a). This mantle unit has been described across many areas in Valles Marineris including Melas, often identified as

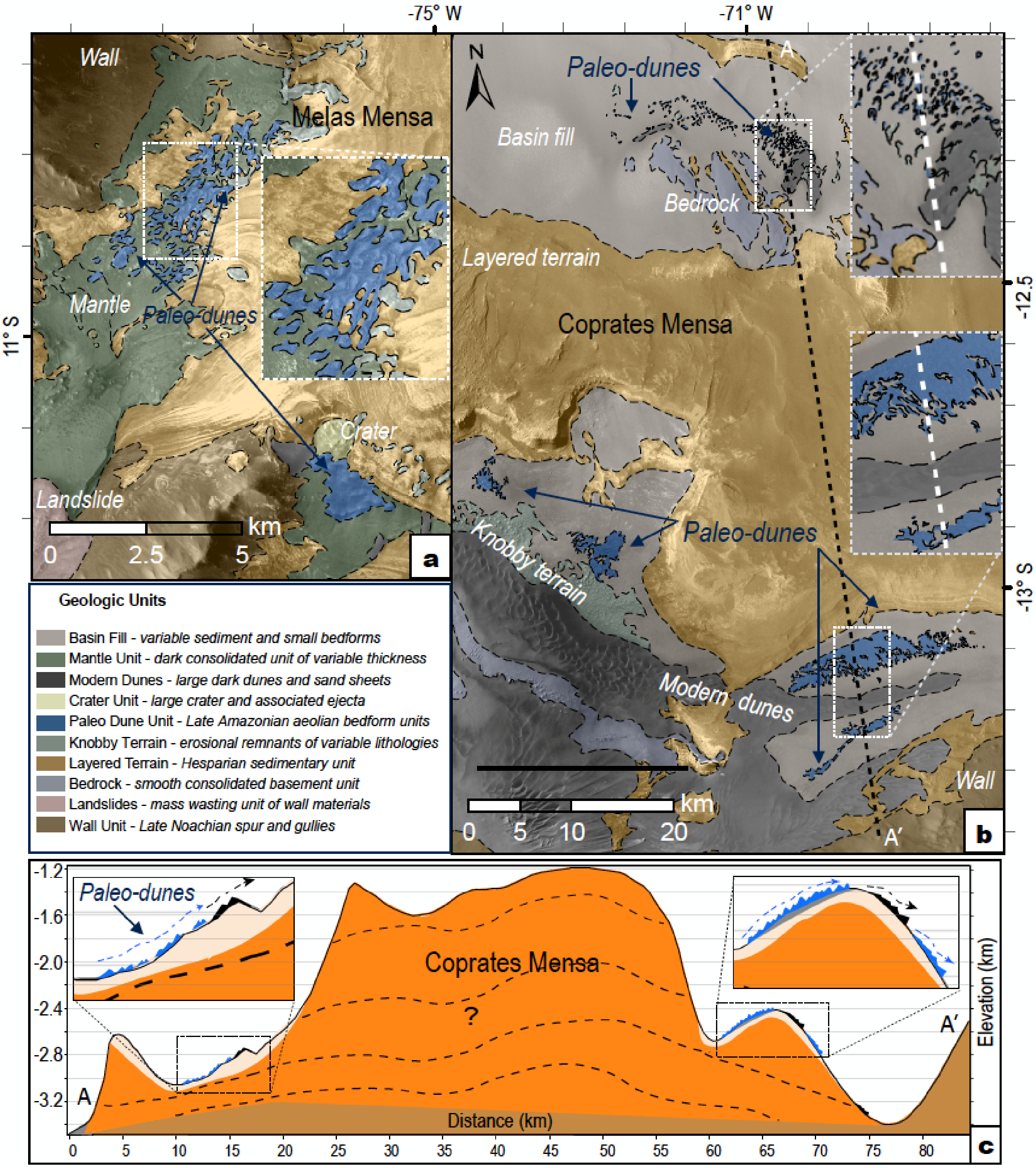

Figure 4. Geologic maps of the (a) Southwest Melas reentrant canyon and the (b) central basin of Melas Chasma. Geologic unit colors and descriptions are provided in the legend. Secondary lat/long tick marks are 1/10°. The central area includes a (c) MOLA cross section (black dashed line) displaying topographic context for these units. Unit thicknesses and layer orientations are approximate, and vertical exaggeration is ~20×.

partially mafic-bearing (e.g., high calcium pyroxene) (Malin & Edgett, 2000; Chojnacki et al., 2014a; Liu et al., 2018).

Interestingly, certain zones of the mantle unit on the paleo-downwin18d (southwest) side of the dune field in Fig. 4a show parallel rows of dark resistant ridges spaced 12–40 m (avg. and 1σ: 22±7 m), 0.5–2 m tall (0.5±0.2 m), and oriented perpendicular to the dune field axis (Fig. 3f, S2). This wavelength range is consistent with that of many TAR populations, often cited to be aeolian mega-ripples (Hugenholtz et al., 2017). Many of these transverse features bifurcate then remerge (Fig. S2). In some areas, these landforms appear to onlap paleo-dune surfaces. Based on their spacing, orientation, stratigraphy, and association with the paleo-dunes, these may be remnants of another ancient bedform type, younger than the dunes investigated in this work.

4.2 Coprates Mensa paleo-bedform morphology and geology

Description: Within the central Melas Chasma basin area are several clusters of candidate paleo-dunes (Fig. 4b). These sites flank the central lobe of the massive sedimentary deposit of Coprates Mensa (Fig. 1d). The northern group shows dispersed crescentic to oval-shaped landforms, adjacent to a modern dune field with lee faces oriented to the south (Fig. 5a-5b, 6). The deposits show evidence of erosion and removal of dune strata, where south faces have been fractured and eroded back, notably with the eastern sides more degraded. Evidence for this erosional trend is most apparent in slope maps of central Melas sites (Fig. S1b). The smoother north sides have relatively gentle slopes (5-15°; Fig. S1b), although the bases appear to be partially buried (Fig. S1). South and west sides tend to be steeper (15-25°).

At least five areas along the southern arc of Coprates Mensa host additional groups of these landforms (Fig. 1d, 4b). These features are variable in terms of morphology, density, degree of preservation, and extent of exposure (Fig. 7). While generally aligned north to south (Fig. 5c-5f), candidates on the southernmost margins show more variability in orientations (Fig. 8). Similar to the northern groups, steepest slopes were consistently observed on the south and west sides of a given candidate (Fig. S1c-S1d). The largest mapped deposit (~20-km wide) also has the highest

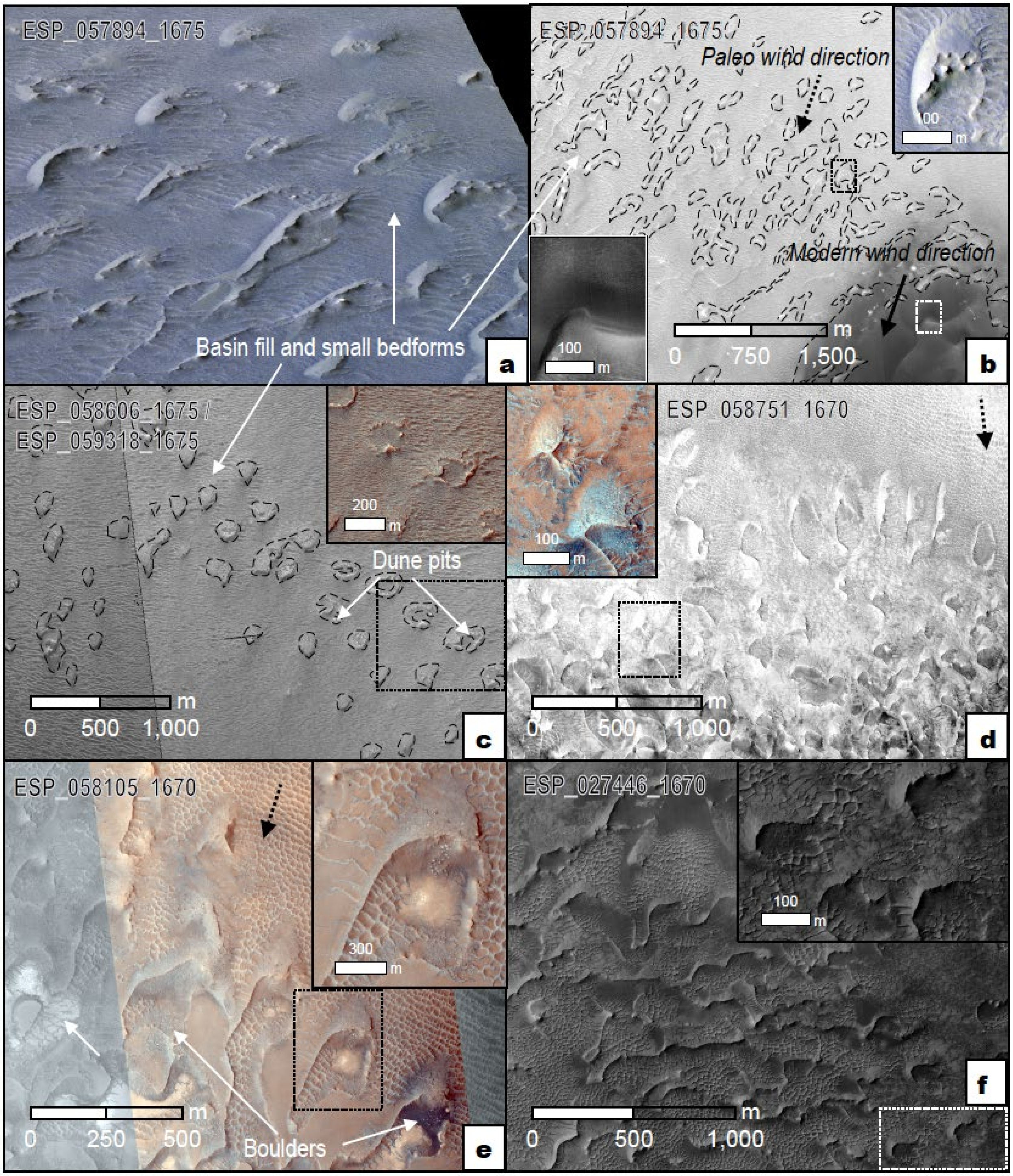

Figure 5. Geomorphology of paleo-dunes in the central basin of Melas Chasma with (b, d, e) interpreted wind directions (dashed arrows). See Fig. 6a for image locations. (a) Oblique color view of one site to the north of Coprates Mensa (field 2891-122) from the southwest (field of view is ~900 m across). (b) Same area as in (a) but showing a wider view of paleo-dune and modern dune units where lee sides or slipfaces show similar orientations. (c) An image to the west where heavily eroded and buried paleo-dunes occur often with prominent pits along crest areas. (d-f) Paleo-dune examples in several fields on the south side of Coprates Mensa (fields 2892-131 and 2886-129). Note the variable basin fill at some locations while others (e) show paleo-barchans sitting directly on sedimentary layered terrain of lower Coprates Mensa.

density of exposures with near-continuous interlocking deposits (Fig. 8). In contrast, in the extreme east of Fig. 1d just ~10 isolated ~150-200-m-long crescentic features are partially buried (also see ESP_027380_1670).

Interpretation: These landforms surrounding Coprates Mensa are interpreted to be ancient duneforms based on the criteria (Section 3.1). Most of these candidates were migrating uphill (Fig. 4c), which further suggests that these are aeolian in origin. The north-south oriented features nearest the mensae are inferred to have been barchan and barchanoid dunes migrating southward. In contrast the southernmost paleo-dunes, oriented northwest to southeast (Fig. 8, S3-S4), are more complex and may indicate spatial differences in the past wind regime(s) (Section 5.1). The notable east-west asymmetry in slopes and paleo-dune shape is partially attributed to differential erosion from eastern winds.

Notable differences are related to the perceived degradation state for some of these landforms compared to the Southwest reentrant paleo-dunes (e.g., Fig. 2, 7). The presence of crescent-shaped deposits of boulders and sediment adjacent to moderately preserved paleo-dunes of similar color and erosional style, suggests that these may have been part of a laterally continuous contemporaneous deposit (Fig. 5, 7, S3). In one area, an elongated paleo-dune limb appears completely eroded back to detrital material (e.g., rocks, sand), whereas summit or remnant crest areas show preservation (Fig.S3a). Small bedforms of dark sand surround or partially bury many

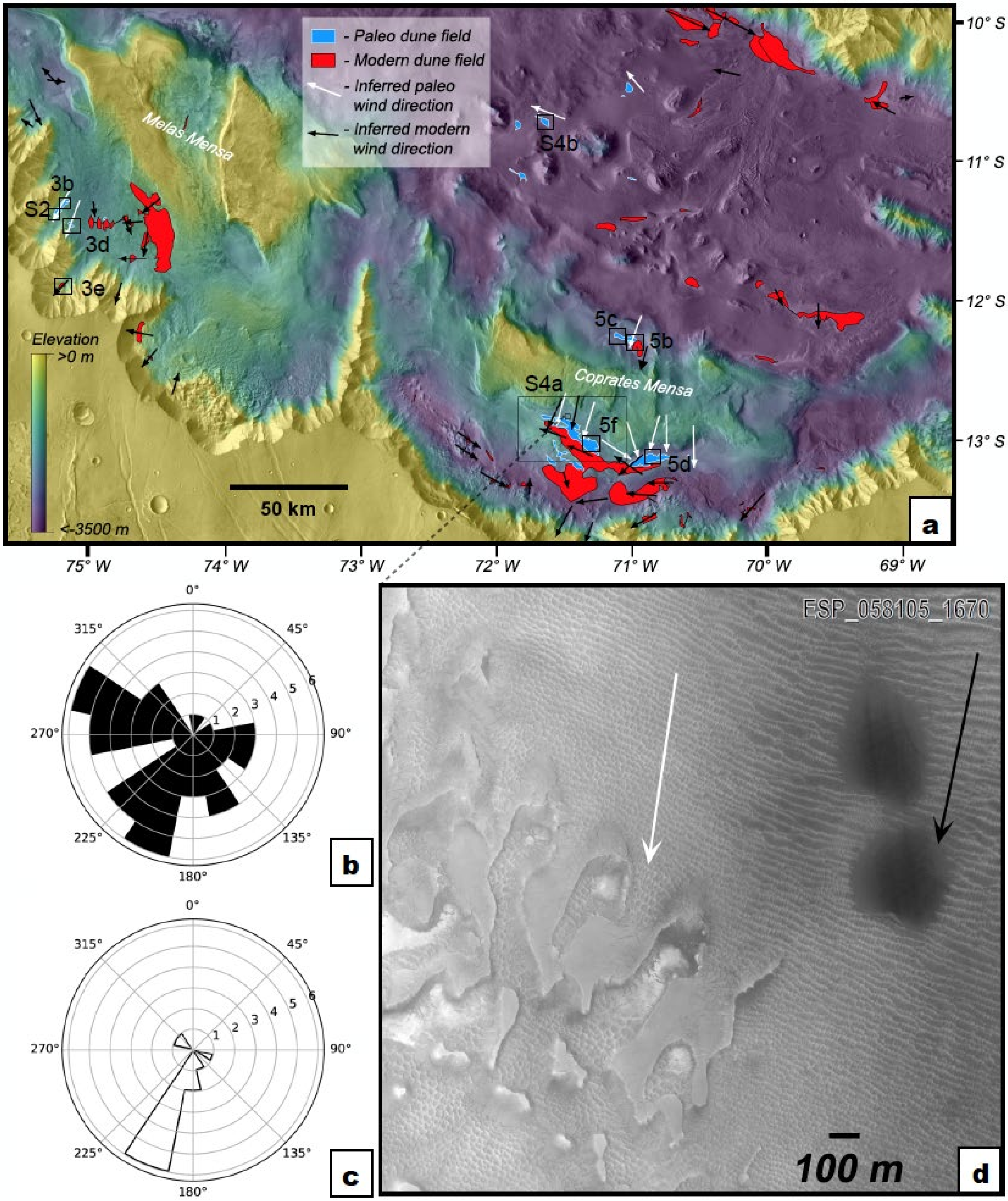

Figure 6. Examples of paleo- and modern wind regimes examples in Melas Chasma. (a) Map of modern and paleo-dune fields and interpreted wind directions (arrows). Base map is THEMIS day-infrared colorized with MOLA elevation. Wind rose diagrams for (b) modern and (c) paleo-dune fields from mapping, indicating downwind transport directions. (d) Examples of adjacent, co-aligned modern (right) and paleo (left) dunes (288.54°E, 12.77°S).

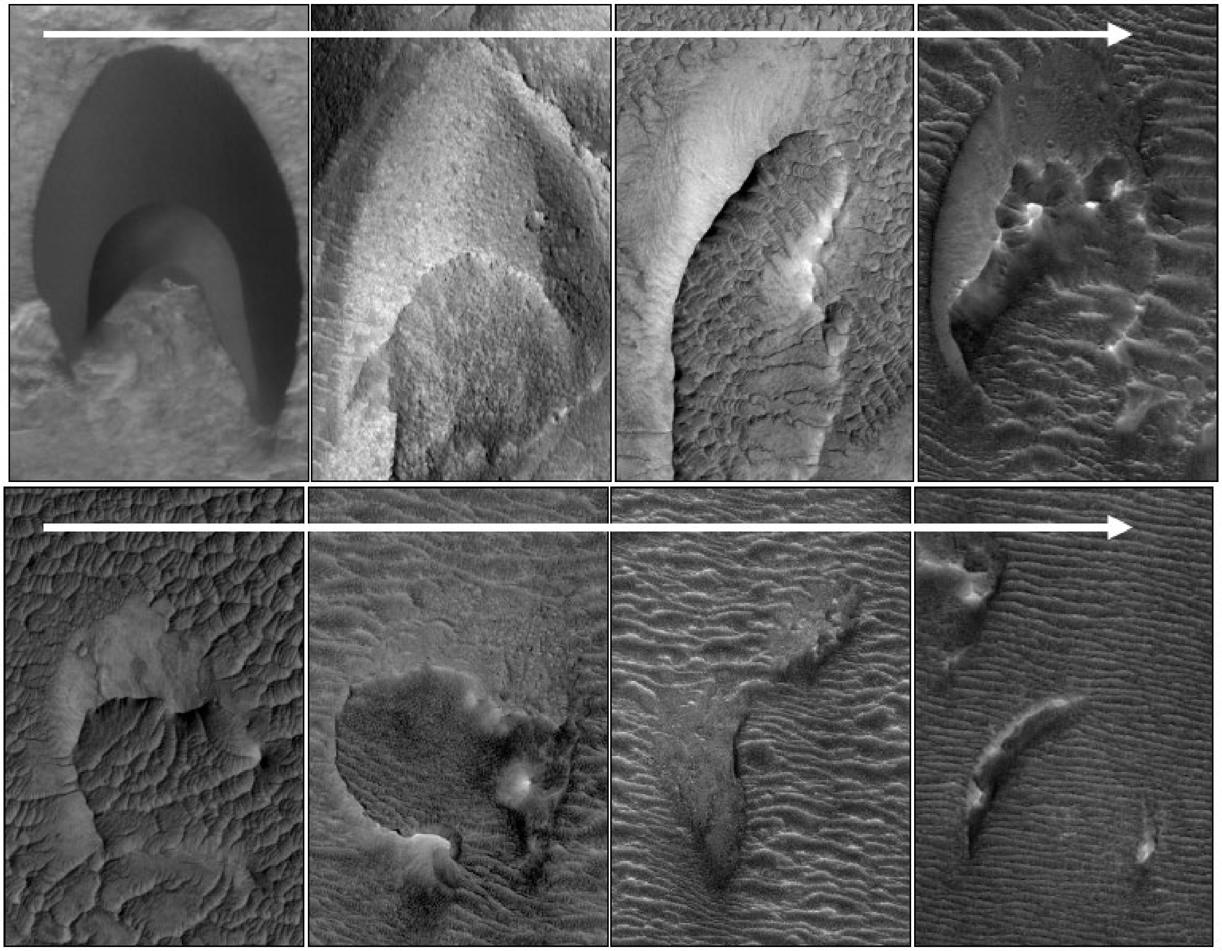

Figure 7. Sequence of dune degradation in HiRISE images at the same scale. All image subsets are 200-meters wide. The top left modern dune example is from Capen crater, whereas the rest are Melas Chasma paleo-dunes. White arrow begins with the modern example and progresses left-to-right and into the lower row to more degraded examples. See Table S3 for image IDs and locations.

paleo-dune areas (Fig. 5e-5f, 8-9). The relatively small (2-4 m spacing) wind ripples, appearing dark-blue to purple in HiRISE color images, appear to be dust-free, potentially mobile bedforms (Fig. 3c, 5f, S3). The occurrence of modern ripples adjacent to paleo-dune talus may indicate that the latter serves as a sand source, providing evidence for sediment recycling. These leeward (south) areas could also be stabilized sand traps. Paleo-dunes and the underlying stratigraphy farthest from the mensa are less exposed due to greater sediment coverage. The basin-fill unit appears to bury up to ~80% of some paleo-dunes, some only identifiable by their protruding summits aligned in a similar manner as eastward examples (Fig. 5a, 5c). In contrast, certain interdune areas nearest Coprates Mensa are largely sediment starved, exposing lower units of the deposit (Fig. 5e, S4).

The central and lee sides of these paleo-dunes are largely eroded away, leaving behind only the lower portions of the stoss slopes and partial remnants of flank and lee bases (Fig. 5c, 5e-5f, 9). Cross sections show that in some cases, the eroded central portions are up to 2 m deeper than the

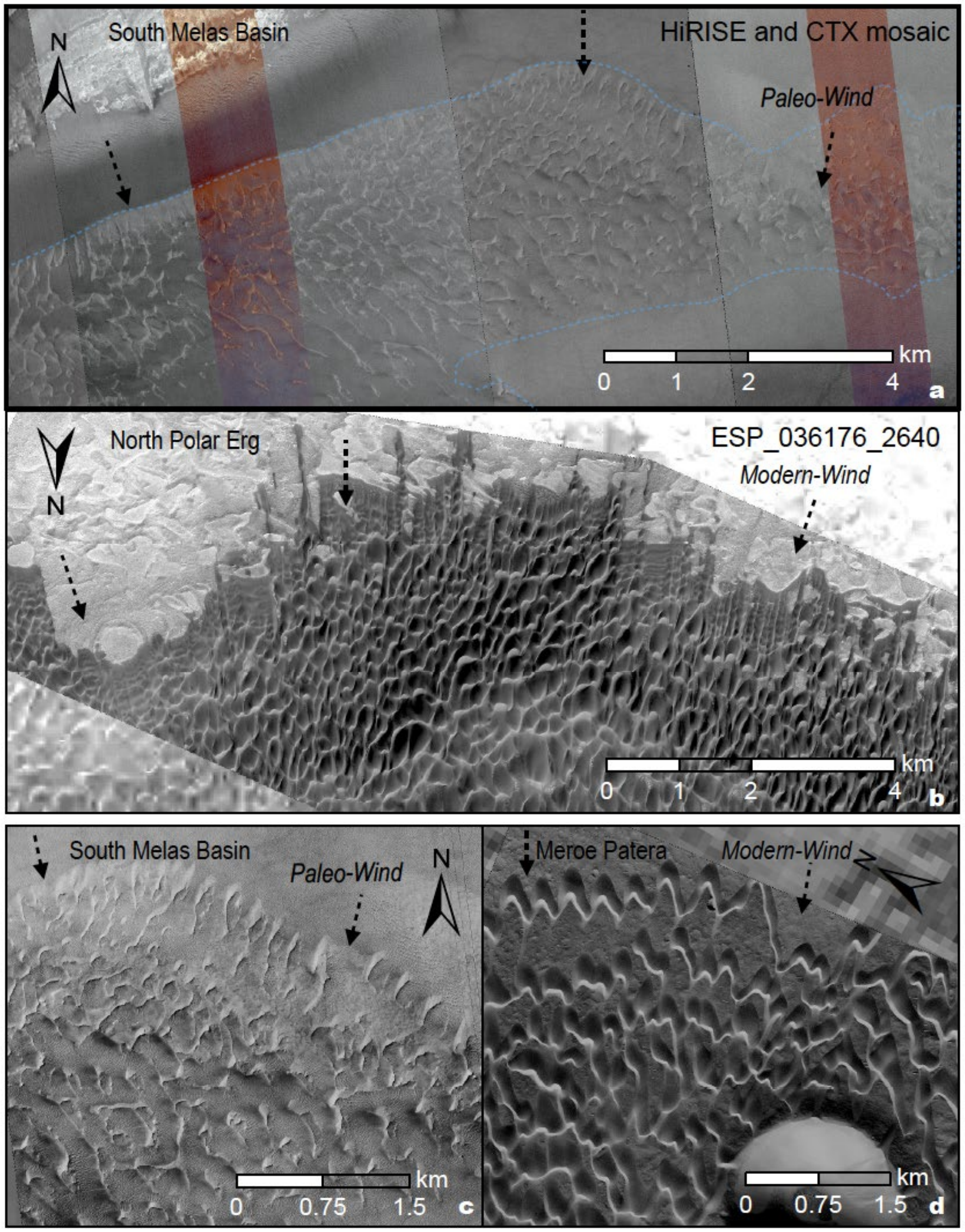

Figure 8. (a) Melas Chasma paleo (289.14°E, 13.09°S) and (b) north polar erg modern dunes (233.8°E, 83.9°N). The cyan dashed lines show the extent of the paleo-dune field. Note the similar symmetry of lateral, parallel rows of barchans that develop at the leading upwind side of these fields that formed under largely unidirectional wind regimes (dashed arrows). In both cases, more complicated dune morphologies occur in downwind areas as topographic complexity and sediment supply both increase. (c) Melas Chasma paleo (289.18°E, 13.08°S; ESP_060729_1670) and (d) Meroe Patera modern dunes (67.7°E, 7.2°N; ESP_042513_1875). Both fields show a leading-edge line of barchans/barchanoid dunes.

surrounding terrain (Fig. 10). These broad pits suggest that the dunes (and the surrounding interdune areas) may have been buried by as much as 2 m of material that became more resistant to erosion than the dune sand, leaving behind a partial cast of the dune as it later became exposed to erosion (Fig. 10)(Day & Catling, 2018).

The geologic map of the central basin area shows the close spatial relationships of paleo-dunes and modern aeolian dunes (Fig. 4b), including one of the larger dune fields in Melas Chasma (Fig. 6a). Geologic cross sections of

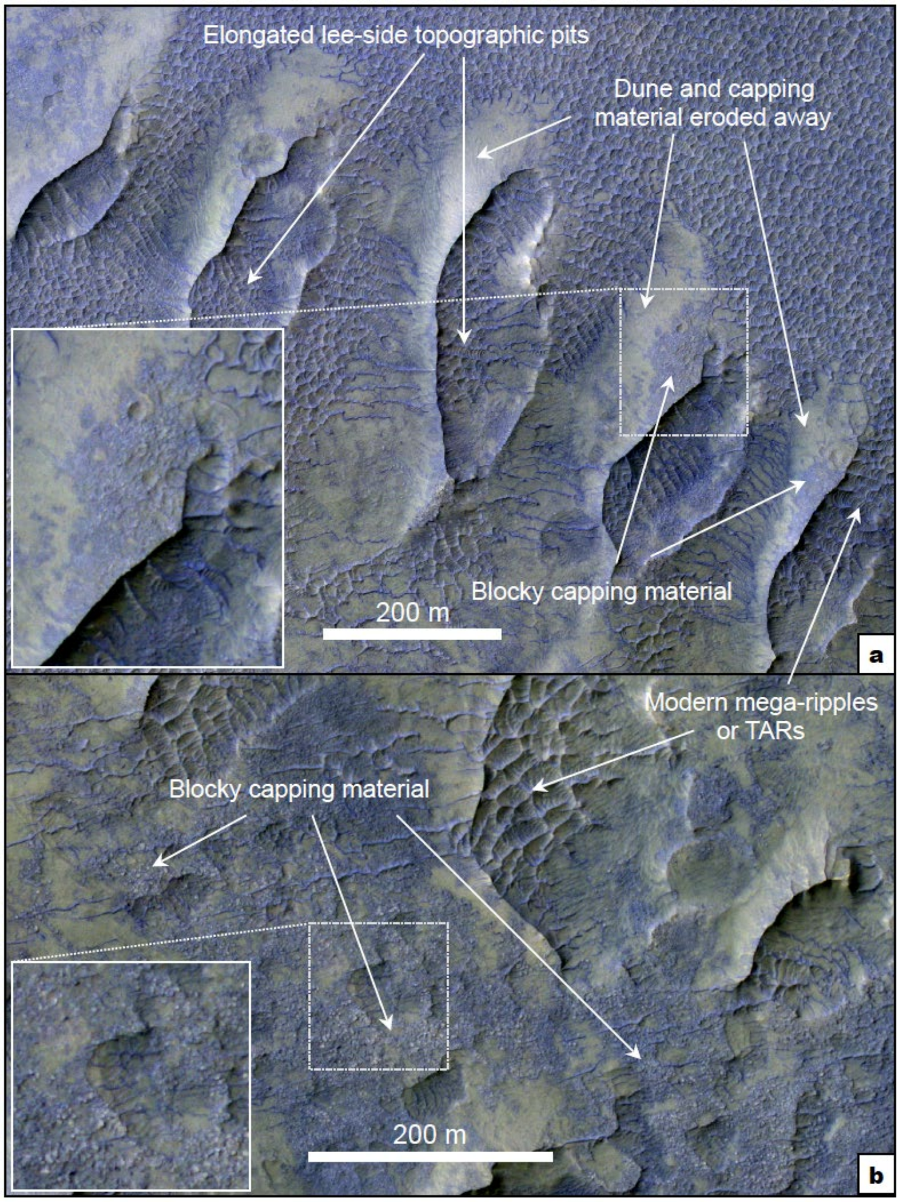

Figure 9. Examples of the paleo-dune geologic units and pits in the south-central areas of Coprates Mensa (289.17°E, 13.07°S). HiRISE (IRB) image ESP_060729_1670. See Fig. 6a for image locations. (a) The leading edge of the largest deposits (see Fig. S3) shows distinct exposures of a blocky capping unit present on stoss, crest, and interdune areas which appears to have been eroded back in some locations. Blueish to violet colors of these units and local bedforms indicate an enhanced ferrous content from mafic minerals, while (tan to brown) smooth areas are likely more ferric enhanced. (b) Interdune areas to the south that show more extensive blocky capping units. Both areas also show lee side topographic pits which are elongated paleo-downwind and maybe dune cast elements.

these areas show most of these deposits are located on the sloping walls of small basins local to the mensa (Fig. 4c). Most of these paleo-dunes appear to have been climbing uphill (migration from north to south up the flank of Coprates Mensa). The modern dune fields (Fig. 4b, S4a) adjacent to (and apparently overlying yet more remains of) the paleo-dune fields here mainly reflect along-slope winds from the east. The mantle unit appears here as a thinner, blocky, gray unit which often caps upper portions of dunes, somewhat distinct from the Southwest reentrant area (compare Fig. 3 to 9).

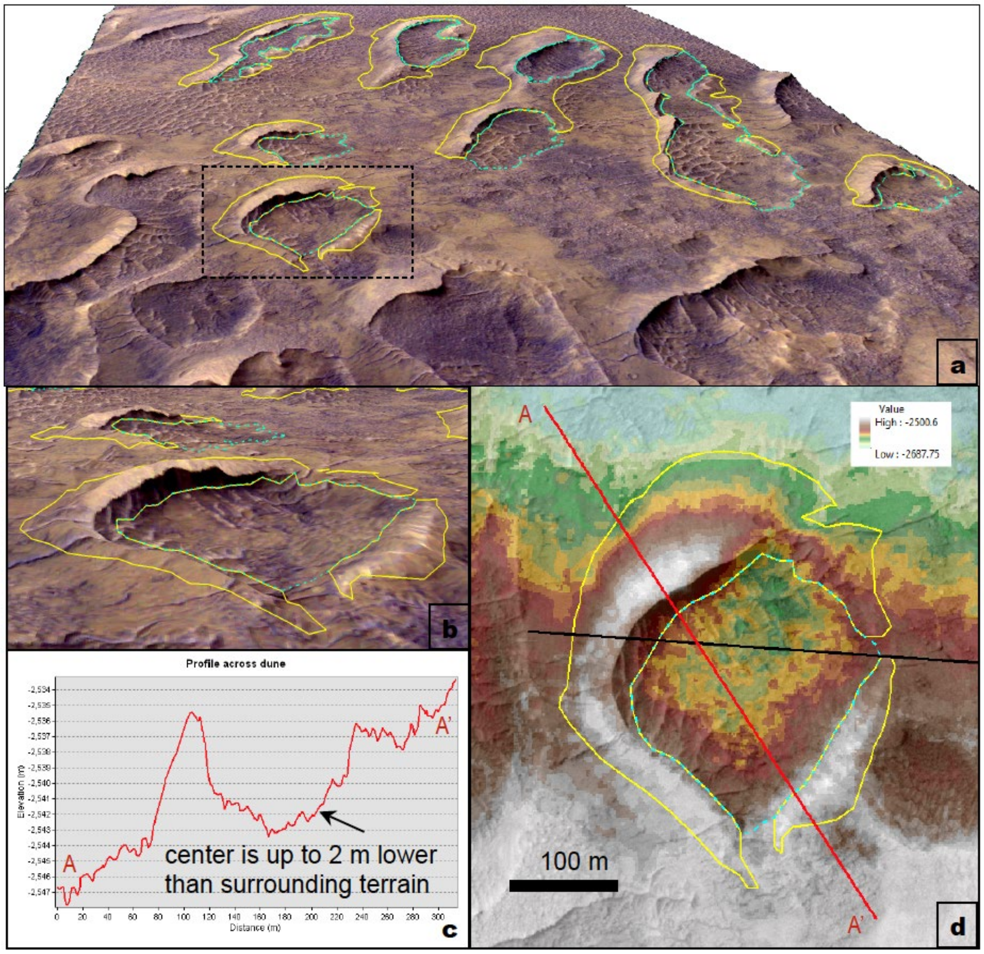

Figure 10. Morphology and topography of paleo-dune pit and casts. (a-b) Oblique view of paleo-dunes south of Coprates Mensa where the field of views are ~1 km and 200 m across. HiRISE ESP_060729_1670 (IRB) with DTM DTEEC_060729_1670_060795_1670_A01 for topography. Location 289.17°E, 13.07°S. (c) Topographic profile showing dunes were on an uphill slope and lee side central pits are several meters deep. (d) HiRISE colorized with elevation showing context for the profile. Note the black line is a data gap.

4.3 North Melas basin paleo-bedform distribution and morphology

Description: Scattered across the north-central basin of Melas Chasma are ~15 sites of candidate paleo-bedforms (Fig. 1a, 6) observed within CTX images, which fulfill some of the proposed criteria. Most of these landforms are heavily eroded, largely buried, and/or lack HiRISE coverage for further investigation. Those that do have high-resolution data coverage show oval to crescentic mounds of consistent orientation that are occasionally fractured and found in groups with similar spacings as other Melas sites (~200-300 m; Table S1). Like the south basin features, these candidates appear eroded with pits on their eastern flanks (Fig. S4b). From their plan-view shapes, apparently the shallower, unfractured slopes are toward the southeast, whereas the steepest slopes are oriented toward the northwest. Some of these northwest-facing slopes are arcuate, seemingly even sloped, and resemble intact slip faces (e.g., inset in Fig. S4b).

Interpretation: These north basin features are inferred to be paleo-dunes like those elsewhere in the chasma (Fig. 7). The abundance of pits and fractures on the southeast (inferred stoss) sides suggests post-lithification abrasion by winds with a strong easterly component. The northwest-facing putative slip faces may have been preserved because they are sheltered from the erosive easterly wind. The inferred northwesterly migration direction contrasts with the south to south-southwestward migration of the south basin paleo-bedforms, but the bedforms are consistent with modern dune fields in the north basin that indicate along-chasma transport to the northwest and southeast (Fig. 6a) (Chojnacki et al., 2014a). Then, as now, bedform morphology and migration appear to have been strongly influenced by local topography.

4.4 Constraints from thermophysical and compositional properties

4.4.1 Thermophysical Properties

Description: Thermal inertia values were derived from the entire fields of seven Melas Chasma paleo- dune sites (Tables 1, S2) and from individual paleo-dunes (averaged) for six of the seven sites (Fig. S5). The similar results from the two methods indicate thermal inertia of the entire field is representative of individual paleo-dunes. To help determine if the paleo-dune fields transect a thermally distinct unit, Table S2 values include adjacent terrain (i.e., the most proximal region of the geologic units directly touching the fields). Paleo-dune thermal inertias are between 166 and 300 TIU, while the adjacent terrain flanking the fields are between 174 and 317 TIU (e.g., Table S2; Fig. 8b), but are typically within 1σ-2σ of one another. Paleo-dunes superposed on layered deposits (Fig. 8b, S5e) are typically more thermally distinct than those located in central basins (Fig. S5c).

Interpretation: These results imply that the paleo-dunes themselves are not strongly cemented nor have a thick amount of sediment coverage. Compositional differences extracted from CRISM (see below), and the moderate albedo of these features (e.g., 0.18 from TES), indicate a uniform dust cover is not likely. Scattered, discrete patches of modern aeolian material (e.g., Figs. 3, 5, S3) probably depress the overall apparent thermal inertia at the 100 m/pix THEMIS resolution. For example, the central Melas (north) site, noted to have widespread sediment coverage (Fig. S8c), has the lowest average TI (166 TIU; Table S2), whereas the Southwest reentrant (north) with less apparent fines has a higher average TI (296 TIU). Given the steep slopes which appear with fractures and meter-scale boulders, we infer many of these paleo-dune surfaces are more consolidated than can be determined from THEMIS analysis. For reference, thermal inertia values of modern dunes in Melas and other locations (Table 1), most likely dominated by unconsolidated very fine to medium sand sizes (62−500 μm), frequently produce comparable THEMIS values (200–400 TIU) (Chojnacki et al., 2014a; Edwards et al., 2018).

4.4.2 Compositional Properties

Description: Compositional analysis was conducted on the one targeted CRISM observation of paleo-dune fields available in the study area (Fig. 11a). CRISM results of the Southwest Melas reentrant paleo-dunes showed a distinct 2 μm absorption with a roll-off toward

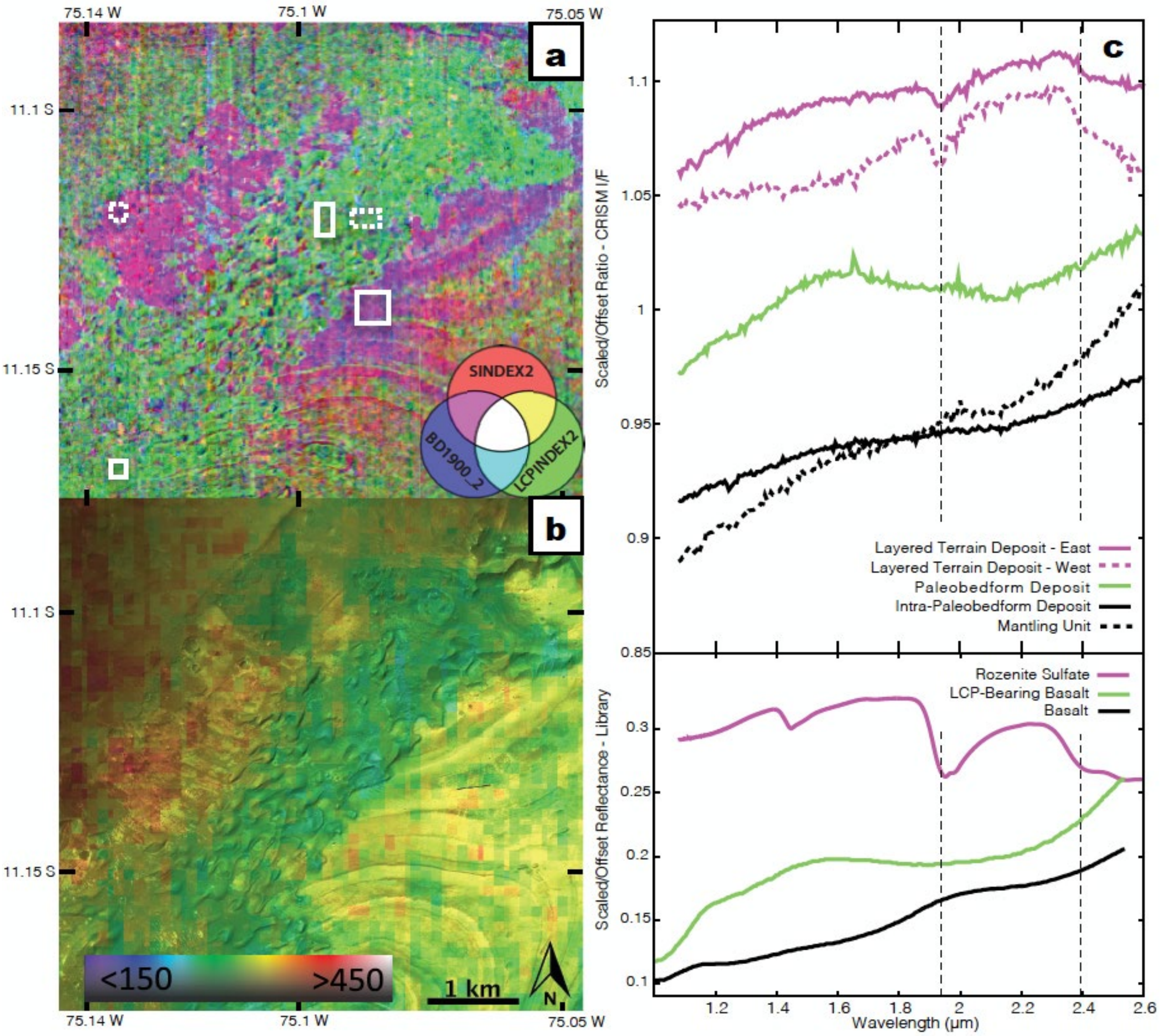

Figure 11. Compositional and thermophysical trends in the Southwest Melas reentrant canyon area (field 2849-111). (a) A parameter map where colors are: R: SINDEX2 to identify strong 2.4 µm band depths associated with hydrated sulfates, B: BD1900_2 to identify 1.9 µm band depths associated with bound H_2O, G: LCPINDEX2 identifies low calcium pyroxene. (inset) A color wheel key where magenta indicates polyhydrated sulfates and green indicates low-calcium pyroxene. CRISM observation FRT0000A3E9. (b) A CTX image colorized with thermal inertia values in units of TIU. Also see Fig. S5. (c) CRISM spectra (top) and corresponding library spectra (bottom) of layered terrain deposits (magenta), paleo-dunes (green), and the mantle (black). Lab spectra are from PDS Geosciences Spectral Library: http://speclib.rsl.wustl.edu/.

1 µm (Fig. 11c). The spectral character of the paleo-dunes does not vary significantly, such that the paleo-dune spectrum is representative of all in the scene. Adjacent mantle unit and interdune area spectra are similar but lack the 2 µm feature and have a more pronounced red slope. In

contrast, spectra of the flanking sedimentary terrain are distinct with 1.9-1.95 μm absorption features, and a drop-off at ~2.35 μm.

Interpretation: The spectra of the paleo-dunes best match a low-calcium, pyroxene-enriched basaltic composition, with a very broad absorption feature centered at 2 μm (Mustard & Pieters, 1989). This is a common spectral character for many modern Martian dunes and aeolian deposits, including some in Valles Marineris (Chojnacki et al., 2014a; Liu et al., 2018), indicating these deposits may have a similar provenance. The mantling unit and interdune spectra are more representative of a typical basalt (Mustard & Pieters, 1989). Spectra of the adjacent layered deposits have absorption features that most closely match that of a polyhydrated sulfate (e.g., rozenite; Bishop et al., 2004), as supported by CRISM parameter maps (Fig. 8a). Collectively, both spectroscopic (e.g., no obvious alteration phases observed) and thermophysical (typically low TI consistent with a weakly consolidated rock) results indicate low degrees of cementation.

4.5 Comparisons with modern aeolian bedforms

The Melas Chasma deposits are remarkably similar to contemporary Martian dunes (Fig. 2, 8). One modern example in Capen crater shows spatial patterns analogous to those in the Southwest reentrant area—both have isolated upwind or flanking barchan dunes that coalesce or link downwind (Fig. 2a vs. 2b, 7). At a broad scale modern examples show similar trends in morphology and overall field shape. For example, relatively symmetric parallel rows of barchans at the upwind edge of fields may develop from a linear sand source under a largely unidirectional wind regime (Fig. 8) (Ewing et al., 2010; Davis et al., 2020). In these cases, more complicated dune morphologies occur in downwind areas likely due to a combination of factors (e.g., dune-dune interactions, variable wind directions or topography). Noticeable differences in dune shapes or areal coverage are also evident with some Melas paleo-dune fields compared to McLaughlin crater modern dunes, although their spacing is comparable (Fig. 2c-2d). The former may be the result of the differential erosion and partial burial of the paleo-dunes.

Bedforms increase in scale with crest-to-crest spacing in a predictable manner that is most apparent for simple crescentic dunes (Fig. 2, 9)(Lancaster, 2009). This well-established relationship reflects both dune dynamics (vertical accretion vs. migration or extension) and sand availability (Lancaster, 1988; Hugenholtz et al., 2012). Figure 12a shows trendlines of height vs. wavelength are generally steepest for modern dunes where relief is maintained. Roughly half of individual Melas paleo-dunes plot atop modern

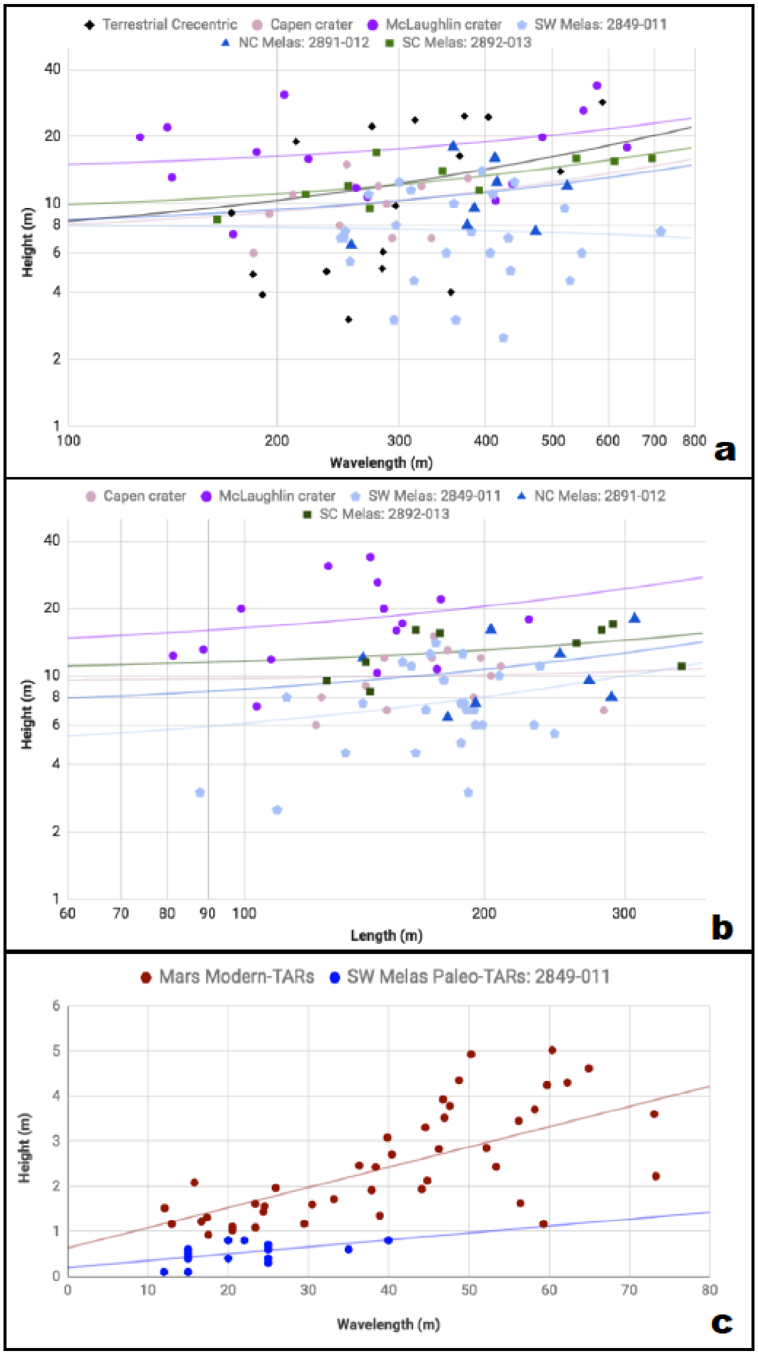

Figure 12. Morphologic comparison for modern and paleo-bedforms. (a) Log-log plot of dune height vs. wavelength for various martian and terrestrial (Lancaster, 2009) dune fields. Compare with Fig. 2. (b) Log-log plot of dune height vs. length for various martian dune fields. (c) Linear plot of height vs. wavelength for paleo-TARs shown in Fig. 3f compared with modern TARs (Geissler and Wilgus, 2017). Note the generally steeper trends for modern bedforms, whereas Melas examples show more modest heights, presumably due to dune crest erosion.

dunes, but many paleo-dune heights are depressed at a given wavelength. Similar trends can be observed between dune length and height (Fig. 12b). Modern TARs also show this relation compared with putative paleo-TARs (Fig. 12c). These depressed heights are attributed to the erosion of crests (e.g., aeolian abrasion, mass wasting) and the burial of dune bases by basin fill, making our height measurements less constrained than well-defined modern examples. Compared with the modern-dune slope-intercept relationships we estimate Melas paleo-dunes lost ~20-50% of their height (or 50-80% was preserved). For instance, the Southwest reentrant average observed height was 7.6 m, but modern dunes with this spacing would yield heights 16.2-m tall, thus implying a height loss of ~50% due to burial of bases or erosion of crests.

5.0 DISCUSSION

5.1 Constraints on paleo-wind regimes and past climates

The preservation of past aeolian indicators, such as the lithified dune fields found in Melas Chasma, provide a useful metric to compare the orientations of nearby contemporary indicators (*e.g.*, wind streaks, dunes) and older (*e.g.*, yardangs) aeolian landforms (Fenton et al., 2015). Significant differences in transport direction might indicate changes in local topography or regional climate, either of which could influence local wind patterns. In contrast, a time-invariant wind regime suggests topographic and/or climatic stability.

Modern dunes in Melas Chasma reflect transport to the south to south-southwest, west to west-northwest, and east to east-southeast depending on the location (Fig. 6). Near the southern chasma walls (Fig. 3e) or flanking Coprates Mensa (Fig. 5b, 6d), the transport is mainly south to south-southwest, likely driven by daytime slope winds constructively interfering with Hadley circulation return flow during southern summer. Mesoscale models of Southwest Melas canyons indicate strong anabatic northeasterly winds (Rafkin & Michaels, 2003), which are consistent these modern dune orientations. Most of the paleo-dunes also indicate transport in this direction (Fig. 6c), suggesting that both local-scale steep topography and the global-scale north-south topographic dichotomy (Richardson & Wilson, 2002) have long controlled circulation patterns in Melas Chasma.

Many modern dunes some distance from the Melas Chasma walls or major mensae reflect along-chasma flows, most often indicating west to west-northwest transport. Paleo-dunes in the north central Melas Chasma floor also suggest transport toward the northwest, with features reminiscent of barchans with slip faces oriented northwest (Fig. S4b). These paleo-dunes, like those identified elsewhere in Melas (e.g., Fig. 3c, 5), are more eroded on their eastern sides, suggesting longstanding enhanced abrasion by easterly winds. It appears that easterly to southeasterly winds of saltation strength have long been common on the Melas Chasma floor, both in constructing dunes and, later, eroding lithified dunes. Similar flows dominate sand transport pathways elsewhere in Valles Marineris (e.g., Fenton et al., 2014). These winds are likely driven, or enhanced, by equatorial easterly flows common on both Mars and Earth (i.e., “trade winds”).

Estimated paleo-dune transport directions largely align with those of nearby modern dunes (Fig. 3d-3e, 5b, 6), albeit there are clear differences in the populations. For example, the difference in wind rose diagrams for modern (Fig. 6b) vs. paleo- (Fig. 6c) dunes is partially due to the greater sampling of the former in other areas of Melas. One possible exception is just south of Coprates Mensa, where paleo-dune morphology suggests transport to the south-southwest, contrasting with adjacent modern dunes to the south that appear to be migrating orthogonally toward the west-northwest (Fig. 6a, S4a). However, a few small modern barchans near the Coprates Mensa southern scarp are migrating southward, parallel to the direction inferred from nearby paleo-dunes (Fig. 6d). It is possible the mensa scarp topography produces nighttime downslope flows (perhaps enhanced by Hadley circulation return flow during southern hemisphere summer) that push sand southward until it encounters dominant along-chasma flows that push sand toward the west-northwest (Richardson & Wilson, 2002; Rafkin & Michaels, 2003), similar to a wind pattern found in a Ganges Chasma dune field (Fenton et al., 2014). The same configuration may have occurred when the paleo-dunes were active.

Although the Melas Chasma paleo-bedform record is incomplete as some aeolian strata have been removed or buried, those paleo-bedforms that were identified do not paint a dramatically different picture than what can be gained from their modern counterparts. The consistency of major sand transport directions over time suggests both local-scale and global-scale topographically enhanced flows have remained directionally invariant over the time period represented by both modern and paleo-bedforms. Dramatic departures from this circulation pattern, such as those that might be produced by equatorial ice accumulation (e.g., Jakosky & Carr, 1985) or major topographic modifications (e.g., glacial erosion, structural changes (Yin, 2012; Gourronc et al., 2014)), are not apparent from the estimated paleo-transport records in Melas Chasma.

5.2 Constraints on paleo-dune deposits age

Dating of modern bedform surfaces has been problematic due to the paucity of unambiguous craters (Bourke et al., 2010). However, based on this absence, Butcher and Fenton (2011) estimated an upper limit crater retention age of 100 Earth years for degraded, high south latitude dune fields. This exposure age still indicates a young surface where ripples and other processes are reworking dune slopes and erasing small craters, albeit at slow rates compared to many Martian dune fields (Banks et al., 2018). Crater statistical analysis of Meridiani Planum coarse-grained plains ripples suggested they were last active between 200–50 ka (Golombek et al., 2010). South Polar and Meridiani examples may be stabilized or at low activity, but bedform surfaces are largely unconsolidated and major lithification of sediments has yet to occur. Melas Chasma paleo-dunes are sparsely cratered (Fig. 3, S2), but such a small crater range (D ~10-20 m) is insufficient for crater counting analyses, as these are likely secondary impacts.

Based on qualitative comparisons between these and global examples of aeolian bedforms (e.g., TARs, degraded South Polar dunes), we estimate these Melas Chasma paleo-bedform sites are much older. Melas paleo-dunes often directly onlap sedimentary layered deposits (Tanaka et al., 2014), providing an upper limit on age. Reconstructed stratigraphy based on mineralogical arguments and crater counts suggest the layered deposits formed throughout the Hesperian into the Early Amazonian period (Flahaut et al., 2010; Fueten et al., 2010; Weitz et al., 2014). However, these ancient deposit surfaces are friable with poor crater retention, suggesting surface exposure ages much younger, perhaps ~100 Ma (Malin & Edgett, 2000). Lateral and vertical erosion by wind abrasion may lead to the ongoing removal and exposure of sedimentary units (Farley et al., 2014).

The presence of modern Melas Chasma dunes and ripples, some of which have been detected to be active today (Chojnacki et al., 2014a; Chojnacki et al., 2018a), indicates floor landforms including paleo-dunes are subject to periods of aeolian erosion (e.g., Fig. 3c, 5b, 6d, S3). Using sediment fluxes of Valles Marineris modern dunes we can estimate abrasion rates of local basaltic bedrock to be 1–26 µm/yr (or m/Myr) (Chojnacki et al., 2018a)—rates would be higher for more friable sedimentary surfaces, such as lithified dunes. Under these average rates of aeolian abrasion, paleo-dunes would not persist very long on the surface unless buried and/or armored from erosion. For example, partially eroded 10-m tall paleo-dunes would likely only persist for another 400 Kyr - 10 Myr, under current conditions. However, this assumes a continual sand supply and sufficient wind energy for saltation, along with an uncertainty about paleo-dune erodibility. Using more conservative, independent abrasion rate estimates for equatorial areas like Meridiani Planum (0.001- 0.01 m/Myr, Golombek et al., 2006), the 10-m tall example paleo-dune would be removed after ~1 Ga.

A possible independent assessment of the hosting paleoclimate for these deposits may be informed from planetary bedform-scaling relationships. Duran Vinent et al. (2019) argued that martian bedforms are scaled by the height of the

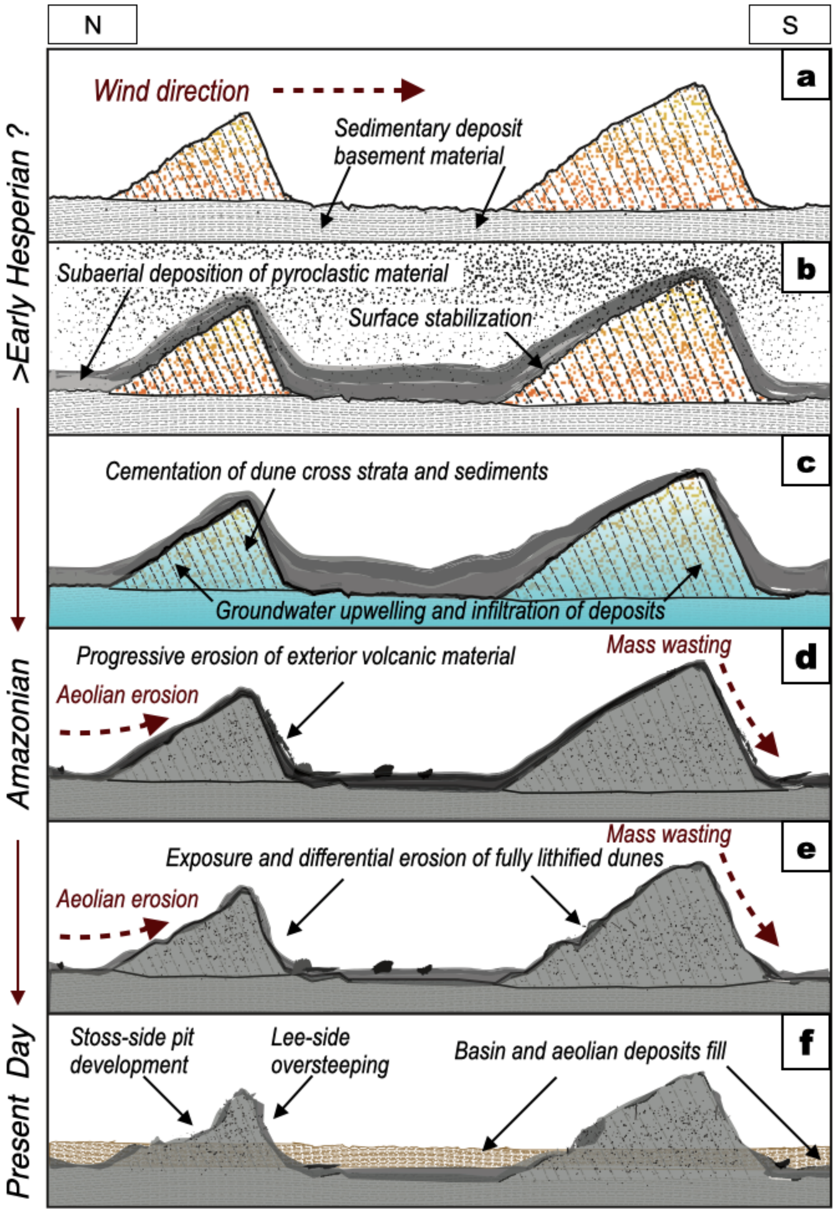

Figure 13. Hypothesized sequence of paleo-dune evolution. (a) Early Hesperian or later unconsolidated dunes migrate mainly southward on Hesperian-aged layered deposits. (b) Subaerially deposited volcaniclastic ash buries dunes then becomes lithified (mantle unit). Dunes are stabilized with morphology preserved. (c) Groundwater upwelling infiltrates dune strata and sediments. Dunes are strongly cemented and lithified. (d) Progressive erosion of exterior mantle unit. (e) Exposure and differential erosion of fully lithified dunes, with degradation of the slip face. (f) Present day: Further erosion and partial burial by Amazonian basin fill of sand, dust, ash, or other materials.

atmospheric viscous sublayer, which is related to both air temperature and density. If correct, their modeling implies significant changes in air pressure would impact the size and spacing of dunes as they form. For instance, dunes may be unable to form at all during periods of low obliquity, when the air pressure is thought to drop considerably (e.g., Toon et al., 1980). Whenever these paleo-bedforms in Melas Chasma formed, they did so under atmospheric conditions not significantly different from those occurring today. If these paleo-dunes formed as long ago as the Early Amazonian or Late Hesperian period, then their size would constrain the corresponding atmospheric pressure to be similar to that of contemporary Mars.

5.3 Proposed sequence of events and implications

The presence and state of these paleo-dunes suggests sequential periods of normal activity, stabilization, cementation, differential erosion and deflation, exposure, and burial. Based on the geomorphic, stratigraphic, and compositional/thermophysical observations, we suggest the following sequence of events to explain the formation and preservation of Melas Chasma paleo-dune deposits:

i. Sometime during the Late Hesperian to Early Amazonian period sand dunes were migrating across Melas Chasma light-toned sedimentary units (Fig. 13a). Decameter mega-ripples or TARs may have been present within the dune fields (Fig. 3f), whether their eventual lithification occurred at the same time is unclear. Bedform sand may have come from a range of possible sources (e.g., wall, sedimentary, or landslide units), but were likely local (Chojnacki et al., 2014b). The driving wind regimes and atmospheric pressure which formed these aeolian systems may not have been drastically different than today.

ii. A substantial amount of material (single to tens of meters) buried the dune fields (Fig. 13b), now recognized as the mantle (Fig. 3) or blocky gray (Fig. 9) units depending on the locations. Based on the spatial variability, thickness, and composition, we suggest these units were subaerially deposited volcaniclastic materials (Kremer et al., 2019) leading to catastrophic burial. Pyroclastic ash and tephra have been proposed for certain Valles Marineris deposits based on their morphology and proximity to the Tharsis volcanic centers (Hynek et al., 2003; Davis et al., 2018). The lithification of ash and glass led to dune stabilization, which were largely preserved as whole stoss-to-lee landforms.

iii. Subsequently a volatile came in contact with the buried sand dunes leading to sediment lithification (Fig. 13c). Groundwater infiltration is the favored process here as it has frequently been invoked for forming numerous Melas floor units some thought to occur in the Amazonian (e.g., Carr, 1995; Weitz et al., 2015). The lack of a CRISM-detected alteration phase does not preclude a cementing agent (e.g., sulfate) or role for groundwater. This lithification event effectively created sandstone, which would later be resistant to slope failure.

iv. Extended periods of persistent erosion led to the partial to complete removal of the volcaniclastic protective shell (Fig. 13d). Mass wasting of steeper faces and aeolian abrasion by sand blasting led to the exposure of the lithified dune surfaces (Fig. 13e), whereas some areas retained mantle materials (Fig. 3d, 9). Throughout these protracted stages, paleo-dune talus and other basin materials buried lower lying dune surfaces (Fig. 7, 13f).

Analogous scenarios have led to the preservation of relict ancient duneforms on Earth as well. For example, a passive eruption of flood basalts infiltrated and partially buried similar, but much larger barchanoid dune fields in Namibia sometime during the lower Cretaceous (133 Ma, Jerram et al., 2000). Similar examples have been documented in Brazil, but include the solidification of dune strata (Waichel et al., 2008). However, these excellent but rare terrestrial analogs are relatively limited in their aerial exposure due to ongoing sedimentary processes or vegetation. In contrast, Melas Chasma possesses extensive paleo-dune fields scattered across the basin floor, where many duneforms and their morphology appear largely intact. The existence and degree of preservation for these examples indicate a difference in landscape evolution over deep time for the two planets.

6.0 CONCLUSIONS

This study involved mapping and characterization of distinct landforms in central Valles Marineris. Based on their morphology (e.g., shape, size, height, and slope distribution), consistent orientation and spacing, relationship to local slopes, and collective properties relative to modern equivalents, we propose these features are lithified aeolian sand dunes. The presence of paleo-dune fractures, pits, and detrital material, along with superposed elements (e.g., craters, small modern bedforms) led to the interpretation that these landforms are relatively ancient. Other key findings include the following:

- Melas paleo-dunes occur stratigraphically above sedimentary layered deposits formed in the Hesperian into the Early Amazonian periods, providing a cap for their age. Other lines of evidence suggest that these features have been exposed on the surface since the Late Amazonian (several Myr – 1 Gyr).
- The paleo-wind regimes inferred from these landforms are largely consistent with local modern wind regime indicators, with some minor exceptions. If there were major shifts in climate, topography, or other contributing factors to regional wind regimes, it was not readily apparent between the two populations of Melas dunes.

- Melas may have experienced multiple episodes of bedform preservation. Decameter parallel rows of dark resistant ridges which have the morphological characteristics of TARs were identified co-located, and superposed on paleo-dunes at one site. Conditions conducive for these bedforms were not drastically different from what can be found today on Mars.
- The geologic processes responsible for the stabilization, preservation, and exposure of paleo-bedforms likely involved: 1) an initial period of fully formed active dunes, 2) a period of rapid bedform stabilization, 3) cementation possibly involving groundwater, 4) progressive erosion via mass wasting and wind, which led to the exposure of the fully lithified duneforms, and 5) partial burial by basin fill.
- Paleo-dunes were found with a range of degradation, where some were heavily eroded or buried while others retained their bulk morphology. The latter end-members of wholly preserved duneforms appear to be more common on Mars compared to the Earth and may signal something important about landscape evolution on that planet.

Valles Marineris paleo-dune fields, with their complex variety of morphologies, degradation states, and variable geologic context, reveal the richness of regional geology. These results provide insight into sediment transport, deposition, and lithification through deep time and are compelling examples of aeolian-driven landscape evolution on Mars.

ACKNOWLEDGMENTS: This research was supported in part by NASA Mars Data Analysis Program Grant 80NSSC21K0040 and the HiRISE/MRO mission. Reviews by Ryan C. Ewing, J. Davis, and the U.S.G.S. helped improve this manuscripts and those efforts are greatly appreciated.

We would like to thank HiRISE operations staff with assistance in targeting and student Kris Akers for DTM production. Supporting information is available in the online version of the paper, including supplemental methodology, tables, figures, and data tables (for Fig. 6b, 6c, 12). All of the data used for this investigation can be found at the HiRISE website (http://hirise.lpl.arizona.edu/) or the Planetary Data System (https://pds-geosciences.wustl.edu/missions/mep/index.htm). Any use of trade, firm, or product names is for descriptive purposes only and does not imply endorsement by the U.S. Government.

REFERENCES CITED:

Ahmed Benan, C. A., & Kocurek, G. A. (2000). Catastrophic flooding of an aeolian dune field: Jurassic Entrada and Todilto Formations, Ghost Ranch, New Mexico, USA. *Sedimentology*, *47*(6), 1069–1080. https://doi.org/10.1046/j.1365-3091.2000.00341.x

Anderson, R. S., & McDonald, R. R. (1990). Bifurcations and terminations in eolian ripples (Vol. 71, p. Eos, 71, 1344.). EOS Trans.

Atwood-Stone, C., & McEwen, A. S. (2013). Avalanche slope angles in low-gravity environments from active Martian sand dunes. *Geophysical Research Letters*, *40*(12), 2929–2934. https://doi.org/10.1002/grl.50586

Bagnold, R. A. (1941). *The Physics of Blown Sand and Desert Dunes*. London: Methuen. p. 265.

Banham, S. G., Gupta, S., Rubin, D. M., Watkins, J. A., Sumner, D. Y., Edgett, K. S., et al. (2018). Ancient Martian aeolian processes and palaeomorphology reconstructed from the Stimson formation on the lower slope of Aeolis Mons, Gale crater, Mars. *Sedimentology*. https://doi.org/10.1111/sed.12469

Banks, M. E., McEwen, A. S., Kargel, J. S., Baker, V. R., Strom, R. G., Mellon, M. T., et al. (2008). High Resolution Imaging Science Experiment (HiRISE) observations of glacial and periglacial morphologies in the circum-Argyre Planitia highlands, Mars. *Journal of Geophysical Research*, *113*(E12). https://doi.org/10.1029/2007JE002994

Banks, M. E., Fenton, L. K., Bridges, N. T., Geissler, P. E., Chojnacki, M., Runyon, K. D., et al. (2018). Patterns in Mobility and Modification of Middle- and High-Latitude Southern Hemisphere Dunes on Mars. *Journal of Geophysical Research: Planets*. https://doi.org/10.1029/2018JE005747

Bishop, J. L., Darby Dyar, M., Lane, M. D., & Banfield, J. F. (2004). Spectral identification of hydrated sulfates on Mars and comparison with acidic environments on Earth. *International Journal of Astrobiology*, *3*(4), 275–285. https://doi.org/10.1017/S1473550405002259

Bourke, M. C. (2010). Barchan dune asymmetry: Observations from Mars and Earth. *Icarus*, *205*(1), 183–197. https://doi.org/10.1016/j.icarus.2009.08.023

Bourke, M. C., Wilson, S. A., & Zimbelman, J. R. (2003). The variability of transverse aeolian ridges in troughs on Mars (Vol. Lunar Planet. Sci., XXXIV, p. Abstract 2090). Presented at the 34th Lunar and Planetary Science Conference.

Bourke, Mary C., Lancaster, N., Fenton, L. K., Parteli, E. J. R., Zimbelman, J. R., & Radebaugh, J. (2010). Extraterrestrial dunes: An introduction to the special issue on planetary dune systems. *Geomorphology*, *121*, 1–14. https://doi.org/10.1016/j.geomorph.2010.04.007

Burr, D. M., Carling, P. A., Beyer, R. A., & Lancaster, N. (2004). Flood-formed dunes in Athabasca Valles, Mars: morphology, modeling, and implications. *Icarus*, *171*(1), 68–83. https://doi.org/10.1016/j.icarus.2004.04.013

Butcher, A., & Fenton, L. (2011). Latitudinal Trends in Morphology and Classification of Southern Martian Dunes. In *42nd Lunar and Planetary Science Conference* (p. Abstract #2091). Houston: Lunar and Planetary Institute. Retrieved from http://www.lpi.usra.edu/meetings/lpsc2011/pdf/2091.pdf

Carr, M. H. (1995). *Water on Mars*. Oxford University Press. p. 248.

Chojnacki, M., Burr, D. M., & Moersch, J. E. (2014). Valles Marineris dune fields as compared with other martian populations: Diversity of dune compositions, morphologies, and thermophysical properties. *Third Planetary Dunes Systems*, *230*(0), 96–142. https://doi.org/10.1016/j.icarus.2013.08.018

Chojnacki, M., Burr, D. M., Moersch, J. E., & Wray, J. J. (2014). Valles Marineris dune sediment provenance and pathways. *Icarus*, *232*(0), 187–219. https://doi.org/10.1016/j.icarus.2014.01.011

Chojnacki, M., Edgar, L. A., Fenton, L. K., & Edwards, C. S. (2018). Morphology of Ancient Bedforms on Mars from the High Resolution Imaging Science Experiment. In *GSA Annual Meeting* (p. Abstract #316568). Indianapolis, Indiana, USA.

Chojnacki, M., Banks, M., & Urso, A. (2018). Wind-Driven Erosion and Exposure Potential at Mars 2020 Rover Candidate-Landing Sites. *Journal of Geophysical Research: Planets*, *123*(2), 468–488. https://doi.org/10.1002/2017JE005460

Christensen, P. R. (1983). Eolian intracrater deposits on Mars: Physical properties and global distribution. *Icarus*, *56*(3), 496–518. https://doi.org/10.1016/0019-1035(83)90169-0

Christensen, P. R., Jakosky, B. M., Kieffer, H. H., Malin, M. C., McSween, Jr., H. Y., Nealson, K., et al. (2004). The Thermal Emission Imaging System (THEMIS) for the Mars 2001 Odyssey Mission. *Space Science Reviews*, *110*(1/2), 85–130. https://doi.org/10.1023/B:SPAC.0000021008.16305.94

Davis, J. M., Grindrod, P. M., Fawdon, P., Williams, R. M. E., Gupta, S., & Balme, M. (2018). Episodic and Declining Fluvial Processes in Southwest Melas Chasma, Valles Marineris, Mars. *Journal of Geophysical Research: Planets*, *123*(10), 2527–2549. https://doi.org/10.1029/2018JE005710

Davis, J. M., Banham, S. G., Grindrod, P. M., Boazman, S. J., Balme, M. R., & Bristow, C. S. (2020). Morphology, Development, and Sediment Dynamics of Elongating Linear Dunes on Mars. *Geophysical Research Letters*. https://doi.org/10.1029/2020GL088456

Day, M. D., & Catling, D. C. (2018). Dune Casts Preserved by Partial Burial: The First Identification of *Ghost Dune* Pits on Mars. *Journal of Geophysical Research: Planets*, *123*(6), 1431–1448. https://doi.org/10.1029/2018JE005613

Delamere, W. A., Tornabene, L. L., McEwen, A. S., Becker, K., Bergstrom, J. W., Bridges, N. T., et al. (2010). Color imaging of Mars by the High Resolution Imaging Science Experiment (HiRISE). *Icarus*, *205*(1), 38–52. https://doi.org/10.1016/j.icarus.2009.03.012

Duran Vinent, O., Andreotti, B., Claudin, P., & Winter, C. (2019). A unified model of ripples and dunes in water and planetary environments. *Nature Geoscience*, *12*(5), 345–350. https://doi.org/10.1038/s41561-019-0336-4

Durrant, L., Balme, M. R., Carling, P. A., & Grindrod, P. M. (2017). Aqueous dune-like bedforms in Athabasca Valles and neighbouring locations utilized in palaeoflood reconstruction. *Planetary and Space Science*, *148*, 45–55. https://doi.org/10.1016/j.pss.2017.10.008

Edgar, L. A., Grotzinger, J. P., Hayes, A. G., Rubin, D. M., Squyres, S. W., Bell, J. F., & Herkenhoff, K. E. (2012). Stratigraphic architecture of bedrock reference section, Victoria Crater, Meridiani Planum, Mars. In *Sedimentary geology of Mars* (pp. 195-). Society for Sedimentary Geology. Retrieved from http://pubs.er.usgs.gov/publication/70004010

Edgar, L. A., Gupta, S., Rubin, D. M., Lewis, K. W., Kocurek, G. A., Anderson, R. B., et al. (2018). Shaler: in situ analysis of a fluvial sedimentary deposit on Mars. *Sedimentology*, *65*(1), 96–122. https://doi.org/10.1111/sed.12370

Edgett, K. S., & Malin, M. C. (2000). New views of Mars eolian activity, materials, and surface properties: Three vignettes from the Mars Global Surveyor Mars Orbiter Camera. *Journal of Geophysical Research*, *105*(E1), 1623–1650. https://doi.org/10.1029/1999JE001152

Edwards, C. S., Piqueux, S., Hamilton, V. E., Fergason, R. L., Herkenhoff, K. E., Vasavada, A. R., et al. (2018). The Thermophysical Properties of the Bagnold Dunes, Mars: Ground-Truthing Orbital Data. *Journal of Geophysical Research: Planets*, *123*(5), 1307–1326. https://doi.org/10.1029/2017JE005501

Ewing, R. C., Peyret, A.-P. B., Kocurek, G. A., & Bourke, M. (2010). Dune field pattern formation and recent transporting winds in the Olympia Undae Dune Field, north polar region of Mars. *Journal of Geophysical Research: Planets*, *115*(E8), E08005. https://doi.org/10.1029/2009JE003526

Ewing, R. C., Lapotre, M. G. A., Lewis, K. W., Day, M., Stein, N., Rubin, D. M., et al. (2017). "Sedimentary processes of the Bagnold Dunes: Implications for the eolian rock record of Mars": Bagnold Dune Field sedimentary processes. *Journal of Geophysical Research: Planets*. https://doi.org/10.1002/2017JE005324

Farley, K. A., Malespin, C., Mahaffy, P., Grotzinger, J. P., Vasconcelos, P. M., Milliken, R. E., et al. (2014). In Situ Radiometric and Exposure Age Dating of the Martian Surface. *Science*, *343*(6169), 1247166–1247166. https://doi.org/10.1126/science.1247166

Fenton, L. K., Michaels, T. I., Chojnacki, M., & Beyer, R. A. (2014). Inverse maximum gross bedform-normal transport 2: Application to a dune field in Ganges Chasma, Mars and comparison with HiRISE repeat imagery and MRAMS. *Third Planetary Dunes Systems*, *230*(0), 47–63. https://doi.org/10.1016/j.icarus.2013.07.009

Fenton, L. K., Michaels, T. I., & Chojnacki, M. (2015). Late Amazonian aeolian features, gradation, wind regimes, and Sediment State in the Vicinity of the Mars Exploration Rover Opportunity, Meridiani Planum, Mars. *Aeolian Research*, *16*(0), 75–99. https://doi.org/10.1016/j.aeolia.2014.11.004

Fergason, R. L., Christensen, P. R., & Kieffer, H. H. (2006). High-resolution thermal inertia derived from the Thermal Emission Imaging System (THEMIS): Thermal model and applications. *Journal of Geophysical Research*, *111*(E12). https://doi.org/10.1029/2006JE002735

Fergason, R. L., Christensen, P. R., Bell, J. F., Golombek, M. P., Herkenhoff, K. E., & Kieffer, H. H. (2006). Physical properties of the Mars Exploration Rover landing sites as inferred from Mini-TES–derived thermal inertia. *Journal of Geophysical Research*, *111*(E2). https://doi.org/10.1029/2005JE002583

Flahaut, J., Quantin, C., Allemand, P., & Thomas, P. (2010). Morphology and geology of the ILD in Capri/Eos Chasma (Mars) from visible and infrared data. *Icarus*, *207*(1), 175–185. https://doi.org/10.1016/j.icarus.2009.11.019

Fortezzo, C. M., Gullickson, A. L., Rodriguez, J. A. P., Platz, T., & Kumar, P. S. (2016). Year 3 Geologic Mapping in Central Valles Marineris, Mars. In *Annual Planetary Geologic Mappers Meeting* (p. Abstract #7038). Houston: Lunar and Planetary Institute. Retrieved from http://www.lpi.usra.edu/meetings/pgm2016/pdf/7038.pdf

Fueten, F., Racher, H., Stesky, R., MacKinnon, P., Hauber, E., McGuire, P. C., et al. (2010). Structural analysis of interior layered deposits in Northern Coprates Chasma, Mars. *Earth and Planetary Science Letters*, *294*(3–4), 343–356. https://doi.org/10.1016/j.epsl.2009.11.004

Golombek, M. P., Grant, J. A., Crumpler, L. S., Greeley, R., Arvidson, R. E., Bell, J. F., et al. (2006). Erosion rates at the Mars Exploration Rover landing sites and long-term climate change on Mars. *Journal of Geophysical Research*, *111*(E12). https://doi.org/10.1029/2006JE002754

Golombek, M. P., Robinson, K., McEwen, A., Bridges, N., Ivanov, B., Tornabene, L., & Sullivan, R. (2010). Constraints on ripple migration at Meridiani Planum from Opportunity and HiRISE observations of fresh craters. *Journal of Geophysical Research*, *115*. https://doi.org/10.1029/2010JE003628

Gourronc, M., Bourgeois, O., Mège, D., Pochat, S., Bultel, B., Massé, M., et al. (2014). One million cubic kilometers of fossil ice in Valles Marineris: Relicts of a 3.5Gy old glacial landsystem along the Martian equator. *Geomorphology*, *204*, 235–255. https://doi.org/10.1016/j.geomorph.2013.08.009

Greeley, R., & Iversen, J. D. (1985). *Wind as a geological process on Earth, Mars, Venus and Titan*. (R. Greeley, Ed.). New York: Cambridge Univ. Press. p. 332.

Grotzinger, J. P., Milliken, R. E., & SEPM (Society for Sedimentary Geology) (Eds.). (2012). *Sedimentary geology of Mars*. Tulsa, Okla: SEPM (Society for Sedimentary Geology). p. 270.

Hugenholtz, C. H., Levin, N., Barchyn, T. E., & Baddock, M. C. (2012). Remote sensing and spatial analysis of aeolian sand dunes: A review and outlook. *Earth-Science Reviews*, *111*(3–4), 319–334. https://doi.org/10.1016/j.earscirev.2011.11.006

Hugenholtz, C. H., Barchyn, T. E., & Boulding, A. (2017). Morphology of transverse aeolian ridges (TARs) on Mars from a large sample: Further evidence of a megaripple origin? *Icarus*, *286*, 193–201. https://doi.org/10.1016/j.icarus.2016.10.015

Hynek, B. M., Phillips, R. J., & Arvidson, R. E. (2003). Explosive volcanism in the Tharsis region: Global evidence in the Martian geologic record. *Journal of Geophysical Research*, *108*(E9). https://doi.org/10.1029/2003JE002062

Jakosky, B. M., & Carr, M. H. (1985). Possible precipitation of ice at low latitudes of Mars during periods of high obliquity. *Nature*, *315*(6020), 559–561. https://doi.org/10.1038/315559a0

Jerram, D. A., Mountney, N. P., Howell, J. A., Long, D., & Stollhofen, H. (2000). Death of a sand sea: an active aeolian erg systematically buried by the Etendeka flood basalts of NW Namibia. *Journal of the Geological Society*, *157*(3), 513–516. https://doi.org/10.1144/jgs.157.3.513

Kerber, L., & Head, J. W. (2010). The age of the Medusae Fossae Formation: Evidence of Hesperian emplacement from crater morphology, stratigraphy, and ancient lava contacts. *Icarus*, *206*(2), 669–684. https://doi.org/10.1016/j.icarus.2009.10.001

Keszthelyi, L., Jaeger, W., McEwen, A., Tornabene, L., Beyer, R. A., Dundas, C., & Milazzo, M. (2008). High Resolution Imaging Science Experiment (HiRISE) images of volcanic terrains from the first 6 months of the Mars Reconnaissance Orbiter Primary Science Phase. *Journal of Geophysical Research*, *113*(E4). https://doi.org/10.1029/2007JE002968

Kieffer, H. H. (2013). Thermal model for analysis of Mars infrared mapping: KRC THERMAL MODEL. *Journal of Geophysical Research: Planets*, *118*(3), 451–470. https://doi.org/10.1029/2012JE004164

Kirk, R. L., Howington-Kraus, E., Rosiek, M. R., Anderson, J. A., Archinal, B. A., Becker, K. J., et al. (2008). Ultrahigh resolution topographic mapping of Mars with MRO HiRISE stereo images: Meter-scale slopes of candidate Phoenix landing sites. *Journal of Geophysical Research*, *113*. https://doi.org/10.1029/2007JE003000

Kocurek, G. A. (1991). Interpretation of Ancient Eolian Sand Dunes. *Annual Review of Earth and Planetary Sciences*, *19*(1), 43–75. https://doi.org/10.1146/annurev.ea.19.050191.000355

Kocurek, G. A., & Ewing, R. C. (2012). Source-To-Sink: An Earth/Mars Comparison of Boundary Conditions for Aeolian Dune Systems. In J. P. Grotzinger, J. P. Grotzinger, & R. E. Milliken (Eds.), *Sedimentary geology of Mars*. Tulsa, Okla: SEPM (Society for Sedimentary Geology).

Kocurek, G. A., Ewing, R. C., & Mohrig, D. (2010). How do bedform patterns arise? New views on the role of bedform interactions within a set of boundary conditions. *Earth Surface Processes and Landforms*, *35*(1), 51–63. https://doi.org/10.1002/esp.1913

Kremer, C. H., Mustard, J. F., & Bramble, M. S. (2019). A widespread olivine-rich ash deposit on Mars. *Geology*, *47*(7), 677–681. https://doi.org/10.1130/G45563.1

Lancaster, N. (1988). Controls of eolian dune size and spacing. *Geology*, *16*(11), 972. https://doi.org/10.1130/0091-7613(1988)016<0972:COEDSA>2.3.CO;2

Lancaster, N. (2009). Dune Morphology and Dynamics. In AnthonyJ. Parsons & AtholD. Abrahams (Eds.), *Geomorphology of Desert Environments* (pp. 557–595). Chapter 18: Springer Netherlands. Retrieved from http://dx.doi.org/10.1007/978-1-4020-5719-9_18

Liu, Y., Goudge, T. A., Catalano, J. G., & Wang, A. (2018). Spectral and stratigraphic mapping of hydrated minerals associated with interior layered deposits near the southern wall of Melas Chasma, Mars. *Icarus*, *302*, 62–79. https://doi.org/10.1016/j.icarus.2017.11.006

Malin, M. C., & Edgett, K. (2000). Sedimentary Rocks of Early Mars. *Science*, *290*(5498), 1927–1937. https://doi.org/10.1126/science.290.5498.1927

Malin, M. C., Bell, J. F., Cantor, B. A., Caplinger, M. A., Calvin, W. M., Clancy, R. T., et al. (2007). Context Camera Investigation on board the Mars Reconnaissance Orbiter. *Journal of Geophysical Research*, *112*(E5). https://doi.org/10.1029/2006JE002808

McEwen, A. S., Eliason, E. M., Bergstrom, J. W., Bridges, N. T., Hansen, C. J., Delamere, W. A., et al. (2007). Mars Reconnaissance Orbiter's High Resolution Imaging Science Experiment (HiRISE). *Journal of Geophysical Research*, *112*(E5). https://doi.org/10.1029/2005JE002605

McGuire, P. C., Bishop, J. L., Brown, A. J., Fraeman, A. A., Marzo, G. A., Frank Morgan, M., et al. (2009). An improvement to the volcano-scan algorithm for atmospheric correction of CRISM and OMEGA spectral data. *Planetary and Space Science*, *57*(7), 809–815. https://doi.org/10.1016/j.pss.2009.03.007

Milliken, R. E., Ewing, R. C., Fischer, W. W., & Hurowitz, J. (2014). Wind-blown sandstones cemented by sulfate and clay minerals in Gale Crater, Mars. *Geophysical Research Letters*, *41*(4), 2013GL059097. https://doi.org/10.1002/2013GL059097

Mountney, N., Howell, J., Flint, S., & Jerram, D. (1999). Relating eolian bounding-surface geometries to the bed forms that generated them: Etjo Formation, Cretaceous, Namibia. *Geology*, *27*(2), 159–162. https://doi.org/10.1130/0091-7613(1999)027<0159:REBSGT>2.3.CO;2

Murchie, S. L., Arvidson, R., Bedini, P., Beisser, K., Bibring, J.-P., Bishop, J., et al. (2007). Compact Reconnaissance Imaging Spectrometer for Mars (CRISM) on Mars Reconnaissance Orbiter (MRO). *Journal of Geophysical Research*, *112*(E5). https://doi.org/10.1029/2006JE002682

Murchie, S. L., Seelos, F. P., Hash, C. D., Humm, D. C., Malaret, E., McGovern, J. A., et al. (2009). Compact Reconnaissance Imaging Spectrometer for Mars investigation and data set from the Mars Reconnaissance Orbiter's primary science phase. *Journal of Geophysical Research*, *114*. https://doi.org/10.1029/2009JE003344

Mustard, J. F., & Pieters, C. M. (1989). Photometric phase functions of common geologic minerals and applications to quantitative analysis of mineral mixture reflectance spectra. *Journal of Geophysical Research: Solid Earth*, *94*(B10), 13619–13634. https://doi.org/10.1029/JB094iB10p13619

Okubo, C. H. (2010). Structural geology of Amazonian-aged layered sedimentary deposits in southwest Candor Chasma, Mars. *Icarus*, *207*(1), 210–225. https://doi.org/10.1016/j.icarus.2009.11.012

Rafkin, S. C. R., & Michaels, T. I. (2003). Meteorological predictions for 2003 Mars Exploration Rover high-priority landing sites. *Journal of Geophysical Research*, *108*(E12). https://doi.org/10.1029/2002JE002027

Richardson, M. I., & Wilson, R. J. (2002). A topographically forced asymmetry in the martian circulation and climate. *Nature*, *416*(6878), 298–301. https://doi.org/10.1038/416298a

Rubin, D. M., & Hunter, R. E. (1982). Bedform climbing in theory and nature. *Sedimentology*, *29*(1), 121–138. https://doi.org/10.1111/j.1365-3091.1982.tb01714.x

Smith, D. E., Zuber, M. T., Frey, H. V., Garvin, J. B., Head, J. W., Muhleman, D. O., et al. (2001). Mars Orbiter Laser Altimeter: Experiment summary after the first year of global mapping of Mars. *J. Geophys. Res.*, *106*(E10), 23689–23722. https://doi.org/10.1029/2000JE001364

Squyres, S. W., Knoll, A. H., Arvidson, R. E., Ashley, J. W., Bell, J. F., Calvin, W. M., et al. (2009). Exploration of Victoria Crater by the Mars Rover Opportunity. *Science*, *324*(5930), 1058–1061. https://doi.org/10.1126/science.1170355

Tanaka, K. L., Robbins, S. J., Fortezzo, C. M., Skinner, J. A., & Hare, T. M. (2014). The digital global geologic map of Mars: Chronostratigraphic ages, topographic and crater morphologic characteristics, and updated resurfacing history. *Planetary and Space Science*, *95*, 11–24. https://doi.org/10.1016/j.pss.2013.03.006

Waichel, B. L., Scherer, C. M. S., & Frank, H. T. (2008). Basaltic lava flows covering active aeolian dunes in the Paraná Basin in southern Brazil: Features and emplacement aspects. *Journal of Volcanology and Geothermal Research*, *171*(1–2), 59–72. https://doi.org/10.1016/j.jvolgeores.2007.11.004

Weitz, C. M., Noe Dobrea, E. Z., Lane, M. D., & Knudson, A. T. (2012). Geologic relationships between gray hematite, sulfates, and clays in Capri Chasma. *Journal of Geophysical Research: Planets*, *117*(E11), E00J09. https://doi.org/10.1029/2012JE004092

Weitz, C. M., Bishop, J. L., Baker, L. L., & Berman, D. C. (2014). Fresh exposures of hydrous Fe-bearing amorphous silicates on Mars: Hydrous Iron Amorphous Silicates on Mars. *Geophysical Research Letters*, *41*(24), 8744–8751. https://doi.org/10.1002/2014GL062065

Weitz, C. M., Noe Dobrea, E., & Wray, J. J. (2015). Mixtures of clays and sulfates within deposits in western Melas Chasma, Mars. *Icarus*, *251*, 291–314. https://doi.org/10.1016/j.icarus.2014.04.009

Williams, R. M. E., & Weitz, C. M. (2014). Reconstructing the aqueous history within the southwestern Melas basin, Mars: Clues from stratigraphic and morphometric analyses of fans. *Icarus*, *242*, 19–37. https://doi.org/10.1016/j.icarus.2014.06.030

Yin, A. (2012). Structural analysis of the Valles Marineris fault zone: Possible evidence for large-scale strike-slip faulting on Mars. *Lithosphere*, *4*(4), 286–330. https://doi.org/10.1130/L192.1